Engineering xxx (xxxx) xxx

Contents lists available at ScienceDirect

Engineering

journal homepage: www.elsevier.com/locate/eng

Micro and Nano Manipulation and Characterization—Review

Optical Microsphere Nano-Imaging: Progress and Challenges

Guangxing Wu [a], Minghui Hong [a,b,c,*]

[a] Department of Electrical and Computer Engineering, National University of Singapore, Singapore 117576, Singapore
[b] Pen-Tung Sah Institute of Micro-Nano Science and Technology, Xiamen University, Xiamen 361005, China
[c] Innovation Laboratory for Sciences and Technologies of Energy Materials of Fujian Province (IKKEM), Xiamen 361005, China

ARTICLE INFO

Article history:
Received 15 April 2023
Revised 10 September 2023
Accepted 17 October 2023
Available online xxxx

Keywords:
Microsphere
Nano-imaging
Virtual imaging
Microsphere compound lens
Engineered microsphere

ABSTRACT

The optical diffraction effect imposes a radical obstacle preventing conventional optical microscopes from achieving an imaging resolution beyond the Abbe diffraction limit and thereby restricting their usage in a multitude of nanoscale applications. Over the past decade, the optical microsphere nano-imaging technique has been demonstrated to be a cost-effective solution for overcoming the diffraction limit and has achieved an imaging resolution of up to about $\frac{\lambda}{6}-\frac{\lambda}{8}$ in a real-time and label-free manner, making it highly competitive among numerous super-resolution imaging technologies. In this review, we summarize the underlying nano-imaging mechanisms of the microsphere nanoscope and key advancements aimed at imaging performance enhancement: first, to change the working environment or modify the peripheral hardware of a single microsphere nanoscope at the system level; second, to compose the microsphere compound lens; and third, to engineer the geometry or ingredients of microspheres. We also analyze challenges yet to be overcome in optical microsphere nano-imaging, followed by an outlook of this technique.

1. Introduction

The invention of optical microscopes is widely recognized as a milestone in the history of scientific advancement that has greatly broadened humanity's knowledge of the microworld [1]. The origins of the optical microscope can be traced back to the simple microscope system invented by Leeuwenhoek in the 1670s [2]. Following an extended era of growth and refinement, the optical microscope has become an indispensable and powerful tool for analyzing micro-objects and has had a profound impact on biological, material, and medical fields [3]. Conventional optical microscopes have many benefits, such as non-invasive imaging, a broad field of view (FOV), a relaxed working environment, and user-friendly operation. Nevertheless, due to the diffraction effect of light waves, the imaging resolution of a conventional optical microscope is confined within the so-called "Abbe diffraction limit", which was discovered by Ernest Abbe in 1873 [4]. Subsequently, other definitions of the diffraction limit, such as Rayleigh's criterion [5], Sparrow's criterion [6], and Houston's criterion [7], were proposed to accommodate different application scenarios in Ref. [8] (pages 257–258). Although there is a slight difference between these criteria, it is clear that conventional lens-based microscopy systems have a limited imaging capacity, making them unable to distinguish objects smaller than roughly half the wavelength of light in ambient air.

Nevertheless, ongoing efforts to improve the resolution of the optical microscope continue to attract significant attention due to the growing demand for applications at the nanoscale, including bio-visualization, for revealing physical phenomena and chemical or pharmaceutical analysis. Researchers have never ceased their efforts to overcome the optical diffraction limit and realize super-resolution optical imaging. To date, a variety of optical imaging techniques have achieved imaging resolutions beyond the optical diffraction limit [9]. These super-resolution microscopy techniques can be broadly classified into two categories: fluorescent super-resolution microscopy and label-free super-resolution microscopy [10]. Over the past few decades, fluorescent super-resolution imaging techniques—including photoactivation localization microscopy, stochastic optical reconstruction microscopy, and stimulated emission depletion microscopy (STED)—have taken significant strides forward in surpassing the optical diffraction limit [11–14]. Three scientists in this field were awarded the Nobel Prize in 2014 due to their pioneering work. Thus far, the resolution of the most advanced fluorescent super-resolution microscopy, such as MINSTED and MINFLUX, is approximately 1 nm [15–17]. Despite its outstanding resolution capabilities, the fluorescent microscope can have negative effects on samples due to the toxicity of the

* Corresponding author.
E-mail address: elehmh@xmu.edu.cn (M. Hong).

https://doi.org/10.1016/j.eng.2023.10.019
2095-8099/

fluorophores and high-power laser pulses. The use of labeling fluorescent dyes may alter the physicochemical properties of biological samples in some cases, resulting in imaging results that do not accurately reflect the original state of the samples. In addition, the fluorescent microscope cannot be applied to the many samples that cannot be dyed, such as silicon and metal. Therefore, many label-free super-resolution imaging methods have also been developed, such as hyper-lenses, super-critical lenses, near-field scanning microscopes, microcylinder lenses, and microspheres [18,19]. Although these techniques have not achieved as high a resolution as the fluorescent super-resolution microscope, they serve as an indispensable complement in various areas, such as semiconductor inspection, where the fluorescent super-resolution microscope is not viable or does not work effectively.

Among these label-free super-resolution imaging techniques, the optical microsphere nanoscope has gained popularity as a promising nano-imaging scheme because of its label-free and real-time imaging capabilities at the nanoscale, as well as its cost effectiveness [20,21]. The microsphere nanoscope leverages the principle of virtual/real imaging magnification by positioning a microsphere on the sample surface to produce an enlarged image of the nanostructures on the sample surface, as illustrated in Fig. 1, which can subsequently be further magnified by means of a conventional optical microscope above the microsphere. Benefiting from the two-cascaded magnification mechanism, nanostructures with feature sizes beyond the optical diffraction limit can eventually be resolved. To date, significant progress has been made in the microsphere nano-imaging technique. These developments of the optical microsphere nanoscope include studying the underlying super-resolution mechanisms, using different immersion media, changing the materials and geometries of microspheres, realizing the locomotion of microspheres, exploiting plasmonic substrates, pairing the microsphere with different microscopes (i.e., fluorescence microscope, confocal microscope, interference microscope, etc.), assembling a microsphere compound lens (MCL), extending the applications of microspheres, and so forth. Several good review papers have comprehensively introduced this progress [22–25].

Considering the ongoing developments in the microsphere nano-imaging technique, some of the latest advancements in this field are introduced in this article. Furthermore, we aim to review the advances in the microsphere nanoscope from another perspective by classifying the developments into two broad categories: developments at the system level and developments at the microsphere lens level, as shown in Fig. 1. At the system level, improvements to all components of the microsphere nanoscope system are included, except for the microsphere lens itself. Typical examples of these components are the illumination source, immersion medium, sample substrate, microsphere holders, and the type of microscopes being paired with microspheres. At the lens level, we focus on direct modifications of the microsphere lens itself, such as changing the composition and geometry of the microspheres and using an MCL rather than a single microsphere. In our opinion, the microsphere lens itself is the soul of the microsphere nanoscope, so to speak, and is worthy of receiving more attention. To highlight the developments at the microsphere lens level, improvements related to the microsphere lens are discussed separately from developments at the system level, which is also what distinguishes this article from other review papers. We aim to offer researchers in this field an alternative perspective to examine the developments in this area and, if possible, provide some inspiration.

The contents of this review are organized as follows. In Section 2, the fundamental physical mechanisms of the microsphere nanoscope are outlined; this is followed by the developments of the microsphere nanoscope at the system level. Developments at the system level include using plasmonic substrates, realizing the locomotion of microspheres, using liquid/solid immersion, and pairing the microsphere with different types of microscopes. Diverse applications of the microsphere nanoscope are also discussed in this section. Sections 3 and 4 introduce the developments of the microsphere nanoscope at the lens level, including the MCL and the engineered microsphere. More specifically, Section 3 summarizes different approaches for assembling an MCL and discusses the superiority of MCLs over a single microsphere in nano-imaging. In Section 4, diverse engineered microspheres are introduced. The specific engineering techniques and consequent enhancements to the imaging capabilities are presented in detail. Then, challenges faced in the field of microsphere nano-imaging are analyzed, followed by the prospects of this technique in Section 5. Finally, a summary of the optical microsphere nano-imaging technique is presented in Section 6.

2. Progress in single microsphere nano-imaging

In this section, we will start with the discovery of the phenomenon of microsphere nano-imaging. Experimental results are presented to highlight the key features of optical microsphere

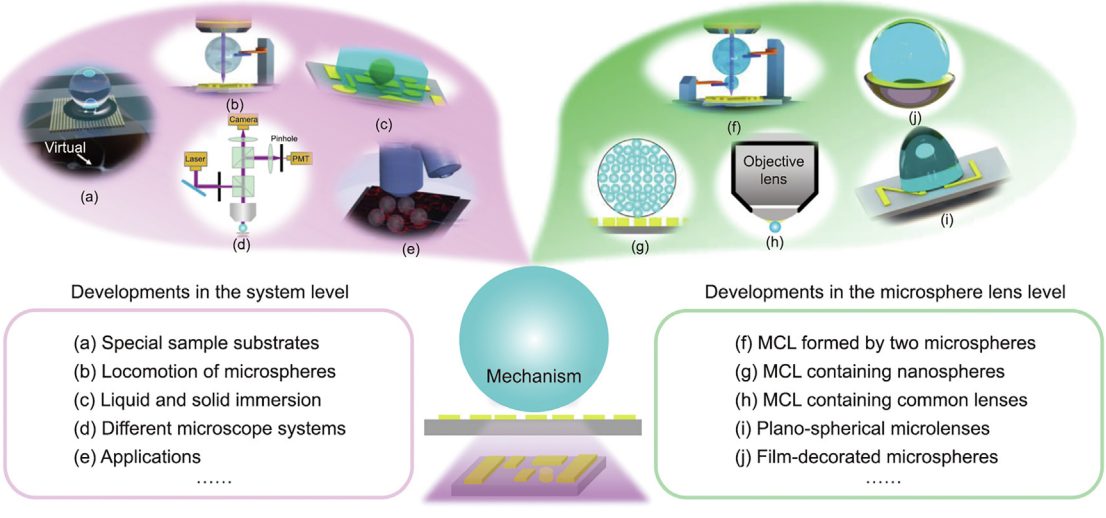

Fig. 1. Schematic of optical microsphere nano-imaging and its developments, which are classified into two broad categories: (a–e) developments at the system level and (f–j) developments at the microsphere lens level. Parts (a) and (e) respectively reproduced from Refs. [26,27] with permission.

nano-imaging, followed by a discussion of the underlying physical mechanisms. Then, techniques to support the locomotion of microspheres are introduced. Two technical approaches to improve or extend the imaging ability of a single microsphere are summarized. Finally, targeted applications of the optical microsphere nanoscope and the current industrialization progress of this technology are introduced.

2.1. Discovery of microsphere nano-imaging

Although the basic interactions between light and micro/nanoparticles were thoroughly studied and understood through Rayleigh scattering theory and Mie scattering theory a long time ago, the experimental discovery of microspheres' unique capability to manipulate light can be dated back to the year 2000 [28–30]. At that time, the semiconductor industry was booming, which led to the development of related technologies and industries. In silicon chip fabrication procedures, wafer cleaning is a critical step, and researchers started to introduce the emerging laser technologies to handle this task. Substantial experimental efforts were devoted to removing the micro/nano-particles on silicon wafers using intense laser pulses. However, removing particles with this technique had significant adverse effects, as it often resulted in micro/nano-holes in the wafer after the cleaning. In particular, researchers found that some generated holes had feature sizes beyond the optical diffraction limit, which sparked intense interest [31]. Scientists conducted many theoretical and experimental studies to reveal the physical mechanisms of this phenomenon. Eventually, the scattered light field of spherical micro/nanoparticles calculated using Mie scattering theory was found to perfectly explain the phenomenon [24,32]. It was found that the scattered field of a spherical particle varies according to its refractive index and size parameter $q = \frac{2\pi R n_m}{\lambda}$, where R, n_m, and λ are the radius of the particle, the refractive index of the environment, and the light wavelength, respectively. When $R << \lambda$, the scattered light field of the spherical particle is very similar to the radiated light field from an electric dipole, which coincides with Rayleigh scattering theory. As the size parameter increases, the distribution of the scattered light field gradually changes from a symmetrical pattern in the forward and backward directions to an asymmetrical jet-like pattern with extremely enhanced light intensity. The full width at half maximum (FWHM) of this optical nanojet is very close to the optical diffraction limit when the diameters of the particles are as small as several micrometers. Meanwhile, the maximum optical field intensity in the photonic nanojet is enhanced by 10–100 times compared with the incident light intensity. This enhancement, in association with the ablation threshold effect of silicon material, leads to the formation of holes with feature sizes beyond the optical diffraction limit [33].

Inspired by the outstanding light-focusing ability of spherical micro/nano-particles, researchers inferred that such particles can also magnify and image nanoscale objects based on the reciprocity principle of light propagation. This hypothesis was experimentally demonstrated by Wang et al. [21] in 2011. In their experiments, the researchers positioned silica microspheres with diameters ranging from 2 to 9 μm on the imaging sample under a conventional white light optical microscope, as shown in Fig. 2(a). They found that patterns with feature sizes beyond the resolving capability of a conventional optical microscope could be discerned with the assistance of silica microspheres. In particular, approximately 50 nm holes in an anodic aluminum oxide (AAO) sample were resolved by the optical microsphere nanoscope under white light illumination, as shown in Fig. 2(b), demonstrating the extraordinary nano-imaging ability of the optical microsphere nanoscope. An overall physical picture of the microsphere nano-imaging process can be simply described using the principle of virtual imaging magnification. As illustrated in Fig. 2(c), the microsphere on the object surface can generate an enlarged virtual image of the nanostructure. If the image size of the nanostructure after the magnification of the microsphere is within the resolution limit of an objective lens in a conventional microscope, the nanostructures can be distinguished by the whole setup. Owing to the outstanding nano-imaging and magnification ability of microspheres, the imaging resolution of a conventional microscope can be upgraded several times.

However, the virtual imaging magnification principle is only a phenomenological explanation and cannot clarify how a microsphere can magnify the image of a nano-object with less blurring compared with an objective lens in a conventional optical microscope. To study the fundamental physical origins of the super-resolution imaging capacity of microspheres, many experimental and theoretical studies have been carried out [38–40]. These experiments have revealed two factors that significantly affect the imaging resolution of microspheres: namely, the size of the microsphere and the type of sample. As the first factor, the imaging resolution of the microsphere is strongly dependent on its size. According to experimental observations and simulations, 4–10 μm microspheres exhibit the best imaging resolution [35,41]. Coincidentally, the magnification of the microsphere, which may indirectly affect the imaging resolution, varies with its diameter as well. The magnifications of 4–10 μm microspheres are greater than those of microspheres with bigger diameters, as displayed in Fig. 2(d).

As the second factor, the imaging resolution and magnification differ when the materials or structures of the samples are changed. Wang et al. [21] demonstrated that a gold coating layer on an AAO sample can simultaneously enhance the resolving power and increase the magnification. The magnification factor for a grating sample is about 4×, which is increased to about 8× for the AAO sample. Shi et al. [42] reported that low-contrast hexagonally close-packed polystyrene nanoparticle arrays with a diameter of 250 nm could only be distinguished when they were deposited with a layer of 30 nm silver (Ag) film. The bare polystyrene nanoparticle arrays could not be resolved by the microsphere nanoscope. Cao et al. [43] found that the resolution of Ag nanostructures is higher than the resolution of those made of gold (Au) and chromium (Cr). The resolution enhancement in metallic samples may be ascribed to the localized surface plasmonic resonance effect. Samples made of materials or structures supporting remarkable surface plasmonic resonance can enhance the generation of surface evanescent waves, which carry fine structure information, and thus increase the resolution [44]. However, the deposition of metallic film on the sample surface may change the original properties of the sample. In particular, such resolution enhancements are not suitable for biological samples. To avoid these limitations, researchers have found that placing samples on substrates, which can support and enhance surface plasmon resonance, can achieve similar resolution enhancements. Yang et al. [45] compared the imaging results of 250 nm polystyrene nanoparticles assembled on a glass slide, an Ag-film-coated glass slide, and a high-reflectance dielectric-multilayer-film-coated glass slide. They found that the polystyrene nanoparticle array could only be resolved by a 30 μm barium titanate glass (BTG) microsphere on the Ag film-coated substrate, which was ascribed to the excitation of the surface plasmon polariton modes for period plasmonic near-field illumination. Later, Pei et al. [36] found that the imaging contrast for such nanoparticles can be further improved by assembling them on a Blu-ray disc substrate, which has a multilayer metal/dielectric coating structure, as illustrated in Fig. 2(e). Such nanostructures in the substrate improve the imaging contrast through the enhanced localized electric field adjacent to the substrate and

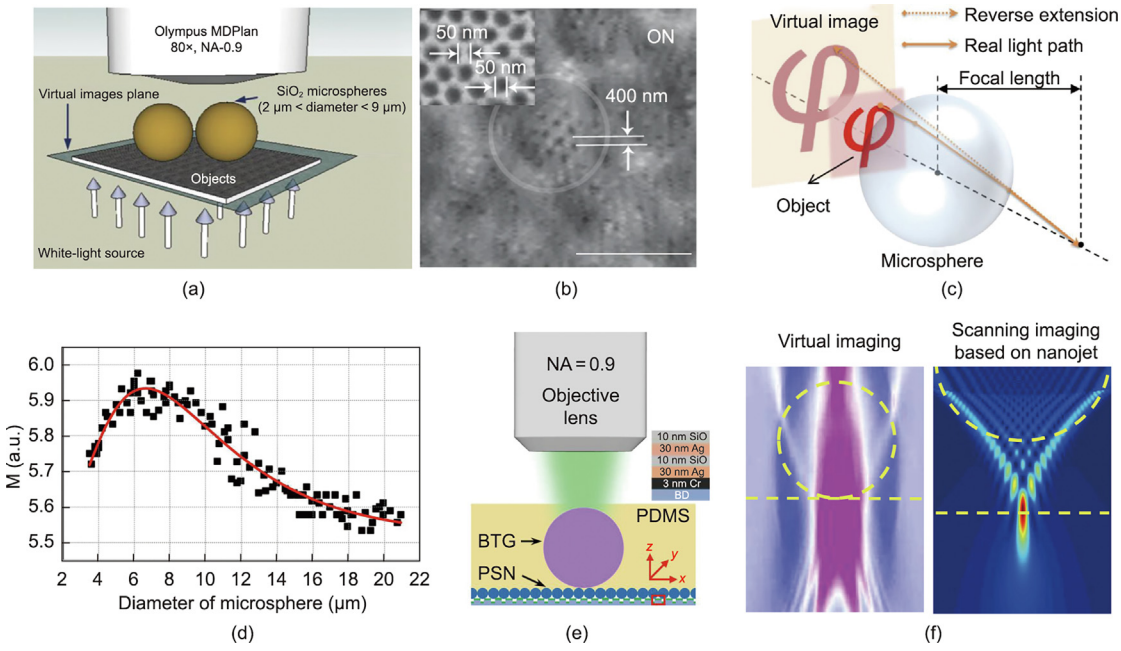

Fig. 2. (a) Schematic of an optical microsphere nanoscope. (b) The imaging result of a gold-coated AAO sample captured by a silica microsphere in air. ON: optical nanoscope. Parts (a) and (b) reproduced from Ref. [21] with permission. (c) Schematic of the virtual imaging principle of the optical microsphere nano-imaging technique. Reproduced from Ref. [34] with permission. (d) Magnifications (M) of microspheres versus their diameters. Reproduced from Ref. [35] with permission. (e) Schematic of using a sample substrate with multilayer metal/dielectric coatings for enhanced microsphere nano-imaging. PDMS: polydimethylsiloxane; NA: numerical aperture; BTG: barium titanate glass; and PSN: polystyrene nanoparticle. Reproduced from Ref. [36] with permission. (f) The difference in illumination conditions between microsphere virtual imaging and microsphere scanning imaging based on the photonic nanojet. Reproduced from Ref. [37] with permission.

samples. Brettin et al. [26] demonstrated that using Au nanodisk arrays with periods of 80 and 100 nm as the sample substrate could increase the imaging resolution up to $\frac{\lambda}{7}$ for fluorescent samples. The observed results were interpreted as the coupling of fluorescence emission to a localized light field confined by plasmonic metasurfaces, which is different from the principle of localized plasmonic structured illumination. These cases that employ nano-plasmonic substrates to enhance imaging resolution may involve slightly different physical processes, but they all exploit the surface plasmon resonance effect and thereby enhance the evanescent wave to some extent.

2.2. Physical mechanism of microsphere nano-imaging

According to these varieties of experimental observations, many hypotheses have been proposed to explain the physical origins of microsphere nano-imaging, including the conversion of surface evanescent waves into propagating waves [46,47], reciprocity between the photonic nanojet effect in focusing and super-resolution imaging [35], resonance mode enhancement [48], the wave theory of virtual image [49], and local enhancement of the numerical aperture (NA) [50]. Next, we provide a brief overview of the fundamental principles of these theories, and then assess their rationality and deficiencies in explaining the optical microsphere nano-imaging mechanism.

The hypothesis that a microsphere possesses the ability to convert near-field evanescent waves into propagating waves was proposed shortly after the experimental discovery of microsphere nano-imaging [51,52]. The evanescent wave conversion theory was previously used to explain the super-resolution imaging of the near-field scanning optical microscopy technique and thus was regarded as a potential explanation for microsphere nano-imaging. Hao et al. [52] suggested that the surface of objects with subwavelength structures can naturally induce evanescent waves in the near-field region based on the angular spectrum theory. Afterward, the rough surface of the sample scatters the evanescent waves, which are subsequently decoupled and converted into propagating waves by the microsphere. The requirements for the distance between the microsphere and the sample surface, as well as the FOV of the microsphere to achieve such a conversion, were theoretically calculated. Later, Ben-Aryeh et al. [46,53] developed a more quantitative model that describes the refraction of evanescent waves at the microsphere boundary and the conditions for the conversion between evanescent waves and propagating waves based on Snell's law. Wave-optics simulations conducted for microspheres in terms of the evanescent wave-scattering process have demonstrated that microspheres can effectively refract evanescent waves and project them into the far field [25]. There is some experimental evidence for this hypothesis [54]. For example, the basis of using metallic samples or nanoplasmonic substrates to improve the imaging resolution of microspheres has often been interpreted as an enhanced evanescent wave due to the surface plasmon resonance effect. Owing to the close relationship between evanescent waves and improved imaging resolution, it is plausible to hypothesize that microspheres can convert evanescent surface waves into propagating waves and thereby obtain images with more detailed information. However, there are three deficiencies of this theory. First, this theory mainly remains within qualitative analysis, and a comprehensive model to describe the excitation of the evanescent wave on the samples, the quantitative spatial frequency distribution of the evanescent wave, the conversion efficiency for different spatial frequencies, and the reconstruction processes of different spatial frequencies in the far field are absent. Second, the theory cannot explain the super-resolution capacity of microspheres on samples that do not support strong surface waves, such as patterns on a silicon substrate and biological samples. Third, some works have reported that microspheres can achieve super-resolution over a long working distance [55]. Over such a distance, the intensity of an evanescent wave will decay significantly, and can almost be neglected. Therefore, the current physical model based on evanescent wave

conversion theory is still far from being the ultimate explanation for optical microsphere nano-imaging.

Another theory widely used to explain the nano-imaging ability of microspheres is the reciprocity relationship between the focusing and imaging processes. In this theory, the imaging resolution of a microsphere is directly associated with the waist of the photonic nanojet produced by the microsphere. Numerous experimental works have conducted simulations of photonic nanojets to explain their imaging results [56–58]. However, the imaging resolution of the microsphere is not equal to the waist width of the photonic nanojet; the former is generally much smaller than the latter according to experimental data. Maslov et al. [41] theoretically demonstrated that the standard resolution defined by the point spread function (PSF) cannot be deduced from the nanojet focusing properties. Therefore, there exists only a certain correlation between the virtual imaging properties and photonics nanojet, rather than a proportional relationship [59]. In addition, it has been suggested that the super-resolution imaging of microspheres can be attributed to the illumination of highly localized light fields focused by the microspheres [25]. It should be noted that most microsphere nano-imaging experiments have been carried out in wide-field illumination conditions with a low-coherent light-emitting diode (LED). Under such illumination conditions, there are no photonic nanojets or other localized light spots focused by the microspheres. Instead, a relatively uniform light field distribution exists at the plane just beneath the microsphere, as illustrated on the left in Fig. 2(f), which is the actual illumination condition for the virtual imaging of microspheres [37]. In fact, in most experiments, the photonic nanojets under the micro/nano-particles, as displayed on the right in Fig. 2(f), are formed under the condition of laser source illumination. The theoretical derivation for the generation of the photonic nanojet was also conducted under the condition of incidence with a monochromatic plane wave. Considering the requirement for laser illumination, a photonic nanojet with a small spot size is more suitable to be applied to modify the performance of a confocal laser scanning microscope, which has already been reported [60]. Therefore, the superior resolving power of the virtual imaging of microspheres is irrelevant with the illumination of a focused light field from the microspheres. The virtual imaging resolution and the waist width of a photonic nanojet are not equivalent and have no straightforward numerical relationship.

Furthermore, considering the spherical geometry, the excitation of the whispering gallery modes and the super-resonance effect in microspheres also is supposed to account for the super-resolution imaging. However, theoretical calculations have proven that the excitation of the whispering gallery mode can only promote the imaging resolution slightly, and the enhancement varies with specific modes [48,61]. Based on such a mechanism, microspheres cannot achieve sub-100 nm resolution under white light illumination. In addition, most commercially available microspheres used for nano-imaging in experiments do not have smooth spherical surfaces; rather, many defects exist on the surface, suppressing the whispering gallery modes in the microsphere. In addition, the sizes of the microspheres have not been selected to support the whispering gallery mode under specific illumination wavelengths in order to achieve nano-imaging. The other theory based on optical resonance to explain the nano-imaging ability of microspheres is the super-resonance effect; this is the result of the constructive interference of partial waves inside a microsphere, which can result in a giant optical field enhancement [40,62]. The super-resonance effect has been theoretically demonstrated to promote the efficiency of converting an evanescent wave on a microsphere into a propagating wave in the far field and thereby improve the imaging resolution [40]. However, the super-resonance effect only occurs for specific values of the Mie q parameter, which has strict requirements regarding the wavelength of illumination light and the working environment of the microsphere [62]. These conditions generally cannot be satisfied in microsphere nano-imaging experiments. Therefore, the excitation of the whispering gallery modes or other optical resonance states may enhance the imaging resolution of microspheres [63], but they are not the radical factors supporting the super-resolving capacity of microspheres.

The wave theory of virtual image has also been developed to describe the virtual imaging processes of microspheres [49,64,65]. In this theory, first, the scattered optical field of the microsphere is calculated by solving Maxwell's equations under the boundary conditions on the surface of the microsphere. Then, the virtual image is calculated by constructing a virtual converging wave using the scattered optical field. Both the Kirchhoff–Helmholtz theorem and the equivalent Fourier-transform formula can be used for the calculation. Bekirov et al. [49] demonstrated that the virtual image of two slits with a width of $\frac{\lambda}{6}$ and a gap between them of $\frac{\lambda}{6}$ is resolved. However, the influence of the sample substrate beneath the microspheres is neglected in this calculation.

Recently, Pahl et al. [50] studied the imaging processes of microsphere-assisted interferometry with a complete simulation model, which considered the practical three-dimensional (3D) conical Köhler illumination, the role of the objective lens, and the light scattering in both the microsphere and specimen. Both the non-resonant and resonant wavelengths for microspheres were simulated and exhibited negligible differences in imaging resolution. The impact of evanescent waves is negligibly small in the simulation because special sinusoidal phase gratings are used as the imaging sample. After excluding the effects of the whispering gallery mode and evanescent wave, the researchers concluded that microspheres positioned adjacent to the sample surface can increase the local effective NA of the whole setup, which is a fundamental factor enabling the super-resolution imaging ability of microspheres. Although this study was conducted for microsphere-assisted interferometry, its results may be extended to the microsphere nanoscope [66]. Direct analysis of the microsphere nanoscope based on this simulation method may help to deepen the understanding of the nano-imaging mechanism.

To summarize, the physical mechanisms behind the super-resolution capacity of microspheres are still under debate thus far. All the factors mentioned above—and/or other factors not mentioned here—could contribute to the super-resolution ability of microspheres under specific circumstances. It is also possible that the synergistic effects of these factors result in the superior resolving power of microspheres. Therefore, this field is still worth exploring further.

2.3. Quantitative analysis of the imaging resolution

Given the complexity of the microsphere nano-imaging mechanism, there is as yet no widely accepted theoretical imaging resolution limit. In this context, it is crucial to quantitatively analyze the resolution of a specific microsphere nanoscope based on experimental results. In many papers on the field of microsphere nano-imaging, the resolution is quantified by the size of the minimum feature that can be resolved in samples. Typical examples include the size of nanoholes in AAO, the line width of Blu-ray disks, the diameter of fluorescent nanobeads, and the edge-to-edge separation distance of two nanostructures [21,27,34,67]. However, resolution values quantified using feature size as a metric exhibit a wide distribution range from $\frac{\lambda}{6}$ to $\frac{\lambda}{17}$, which can be visually observed in the resolution table compiled by Maslov et al. [41] from literature sources. These claimed resolution values are often exaggerated. When the edge-to-edge separation distance of two nanostructures was used to estimate the resolution, it was demonstrated that five-fold exaggeration could occur [22].

To robustly perform a quantitative analysis of the imaging resolution, researchers have suggested two methods: using a standard resolution calibration sample and calculating the PSF of the microsphere nanoscope via the deconvolution method [24,68]. The first method is simple and has been widely used to estimate the imaging resolution of many other optical imaging systems. The second method is based on Houston's resolution criterion, which takes the FWHM of the PSF as the imaging resolution. The PSF of the microsphere nanoscope is calculated from the experimental results via deconvolution. A typical approach to carry out deconvolution in microsphere nano-imaging is function fitting [68]. More specifically, the image is the convolution of the object function and the PSF of the imaging system. If the object function and the image function have already been acquired, the PSF can be calculated by fitting. First, a basic PSF function with some unknown parameters, such as a two-dimensional (2D) Gaussian function with an unknown FWHM, should be properly selected. Then, the convolution result of the object function and the PSF is calculated and fitted to the image function by optimizing the unknown parameters. It should be noted that incoherent and coherent imaging methods have different convolution formulas, which should be chosen accordingly. Once the PSF is determined, the resolution can be estimated with its FWHM. Some published works have exploited this method to quantify the imaging resolution [35,69–71]. For example, Allen et al. [68] used the image of an Au bowtie sample with a 15 nm gap to quantify the imaging resolution and concluded that the resolution of the microsphere nanoscope was $\frac{\lambda}{5.5}$ in that case. Darafsheh et al. [69] reported that the quantified imaging resolution of a microsphere paired with a confocal microscope is approximately $\frac{\lambda}{6}$. Wang et al. [72] reported a quantified imaging resolution of $\frac{\lambda}{8.3}-\frac{\lambda}{6.4}$ for BTG microspheres immersed in water. Most reported imaging resolutions estimated by this method are in the range of $\frac{\lambda}{8}-\frac{\lambda}{6}$. Imaging resolution quantified using the deconvolution method is more plausible and robust than that measured by the minimum feature size. More discussions about the resolution assessment of microspheres can be found in the literature [22].

2.4. Locomotion of microspheres

Although the super-resolution mechanism of microspheres is still controversial, this does not change the fact that microspheres possess extraordinary nano-imaging ability and can be used in extensive applications. In the past decade, significant endeavors have been invested in promoting the comprehensive imaging performance of the microsphere nanoscope. Among this progress, methods to support the locomotion of microspheres have significantly promoted the versatility of this nano-imaging technique in applications.

In the early development stages of the microsphere nanoscope, the microspheres were directly deposited onto the sample surface for nano-imaging; this caused several problems, including the inability to freely locate points of interest for imaging and the contamination or damage of sample surfaces. Since the microspheres could not move over the sample surfaces, this method could only be applied to observe certain periodic samples, such as a Blu-ray disk, AAO, or nanoparticles array, which were frequently presented in the early reported experimental results. Therefore, this microsphere nano-imaging scheme was not very useful in practical applications. Additional measures to facilitate the movement of the microspheres over the sample surface were urgently needed.

To solve this fundamental limitation and realize the locomotion of microspheres, diverse holders were invented to support the precise manipulation of microspheres for nano-imaging. An easily accessible method involves attaching the microsphere to the sharpened tip of a tool—such as the tips of atomic force microscopy (AFM) cantilevers, pipette tips, or surgical needle tips [72–75]. As illustrated in Fig. 3(a), a microsphere is fixed on the tip of an AFM cantilever with optical glue, which has good compatibility with the AFM scanning system, making it easy to acquire images of large-area samples by scanning. In comparison, surgical needle tips or pipette tips are more cost-effective choices, but they require additional procedures to connect the tip with a three-axis moving stage for motion control. To avoid the usage of additional moving stages, specially designed holders that can be directly mounted with the objective lens have been proposed [76]. For example, Huszka et al. [77] designed a holder consisting of a metal frame with a circular opening, to which a cover glass is glued. The metal frame is secured to an adapter, which is fixed onto the objective lens using four metal rods. A microsphere is affixed to the bottom side of the cover glass via a thin layer of optical glue. When the distance between the microsphere and the objective lens is properly adjusted for imaging by shifting the frictional slide along the four rods, the sample under the microsphere can be translated for scanning. Chen et al. [34] designed a similar adapter to connect a microsphere and an objective lens, as illustrated in Fig. 3(b). In their design, the relative distance between the microsphere and the objective lens is precisely controlled with a stepper motor. Moreover, in the development of dielectric immersed microspheres, Darafsheh et al. [68,78] demonstrated that embedding high-refractive-index microspheres in polydimethylsiloxane (PDMS) films can improve the imaging resolution, while also serving as a holder to manipulate the microspheres' motion on samples, as shown in Fig. 3(c). This approach is simple and cost-effective but is limited to high-refractive-index microspheres.

The three aforementioned holders can be categorized as mechanical holders due to their reliance on specialized mechanical elements. Optical tweezers are a completely different type of holder. They were previously widely used for trapping nanoparticles or cells in biological and pharmaceutical fields [79]. In terms of trapping a microsphere with an optical tweezer, it was used in the laser nanofabrication field. For example, in 2008, Mcleod et al. [80] achieved subwavelength nanopatterning using 760 nm polystyrene spheres trapped by a Bessel laser beam in water. With the flourishing development of microsphere optical nano-imaging, optical tweezers have been modified as a microsphere holder in conjunction with the nano-imaging setup. In 2013, Bañas et al. [81] constructed optical tweezers functioning in liquid to trap a customized "tripod" supporting structure, on which a polystyrene microsphere was placed for nano-imaging. The buoyant force of the supporting structure and the polystyrene microspheres in the liquid environment partially balanced their gravity and eased the requirement for the trapping force of the optical tweezers. Later, Michihata et al. [82] proposed more powerful optical tweezers, which can trap a silica microsphere in the air for nano-imaging. As shown in Fig. 3(d), two light sources are employed to construct the optical-tweezer-assisted microsphere nano-imaging system, in which the laser source is used to trap the microsphere and Kohler illumination is used for the surface imaging. Generally speaking, mechanical holders tend to affect the illumination in microsphere nano-imaging because one part of the microsphere must be glued with mechanical elements. This problem does not exist in an optical tweezer scheme. However, the optical tweezer setup can be expensive due to the requirement for additional components, such as the laser source and a high-power objective lens [83]. Moreover, it is challenging to use optical tweezers to trap microspheres with a diameter greater than 10 μm. Thus, optical tweezers and mechanical holders each have their strengths and limitations, and can be utilized as alternative methods based on the specific application requirements.

These holders offer various ways to enable the locomotion of microspheres, which benefits the nano-imaging of microspheres

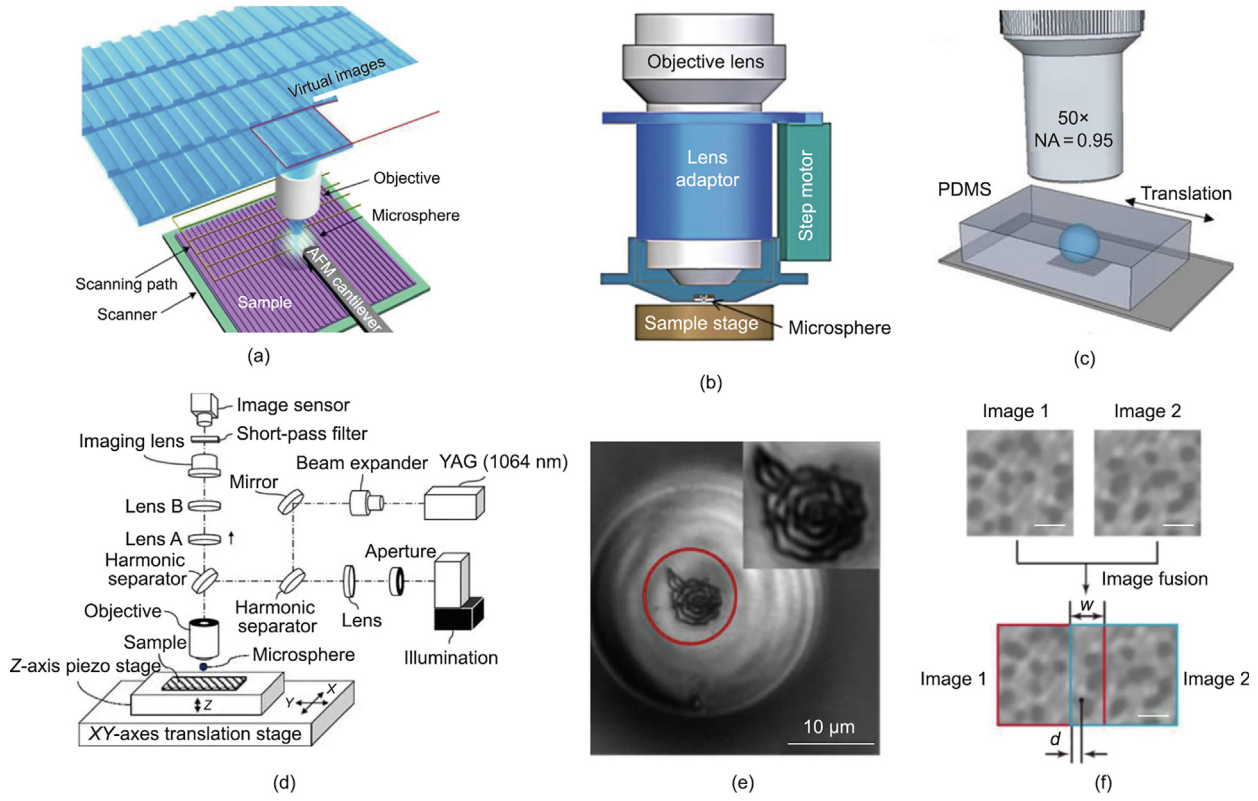

Fig. 3. Diverse microsphere holders: (a) an AFM tip, (b) a lens adaptor for the microsphere, (c) a PDMS membrane, and (d) optical tweezers. (e) Image of a non-periodical nano-rose pattern captured by a microsphere manipulated using a mechanical holder; (f) schematic of stitching two images acquired by a microsphere in adjacent regions of a large-area sample. Parts (a), (c), (d), and (f) reproduced from Refs. [68,72,82,84] with permission, respectively; (b) and (e) reproduced from Ref. [34] with permission.

in two aspects. First, the microsphere can be moved to any point of interest, allowing for the imaging of both periodic and aperiodic samples. As shown in Fig. 3(e), a single nano-rose pattern on a silicon substrate is imaged by a microsphere manipulated using a mechanical holder. Second, the microsphere nanoscope can acquire large-area sample images through scanning and stitching. Thus far, many image stitching schemes have been proposed [72,77,85]. The most straightforward method of image stitching involves recording the locations where each image is captured and merging them in order. However, this simple approach often causes errors due to mechanical vibration or micro/nanoscale deviation in the recorded positions. To ensure correct image stitching, overlapped regions between the two adjacent images must be present during the scanning. Subsequently, these individually scanned images are stitched together through image registration and image fusion. Image-recognition algorithms can also help to improve the results of image stitching. For example, Zhou et al. [84] applied a phase correlation method to align the overlapped region of two images and a linear blending algorithm to fuse the two images. The stitched images, as displayed in Fig. 3(f), validate the effectiveness of these methods. Therefore, the locomotion of microspheres together with effective image stitching methods can be used to achieve super-resolution for large-area samples, which greatly fulfills the demands of many practical applications.

2.5. Microspheres working in dielectric immersion environments

In a conventional optical microscope, oil immersion is a general method to improve imaging resolution; it has also proved to be effective for enhancing the imaging capacity of microspheres. In 2012, Hao et al. [52,86] experimentally demonstrated that the imaging contrast of 3 μm SiO_2 microspheres could be significantly improved by semi-immersing the microspheres in ethanol droplets. The researchers ascribed the imaging contrast improvement to stronger evanescent waves being collected by the microsphere in a liquid environment. Nevertheless, the height of the immersion liquid is not easily controlled, and the imaging characteristics of semi-immersed microspheres may differ in every case. Later, Darafsheh et al. [87] reported that high-refractive-index microspheres (where n = 1.9–2.1) can achieve super-resolution imaging in a fully immersed liquid environment, although this method was considered to be impractical for completely submerged low-refractive-index microspheres. The experimental method for fully immersing the microsphere for imaging is straightforward: spraying a liquid drop to cover the microsphere on the sample surface, as displayed in Fig. 4(a). The experimental results showed that a pattern with a minimum feature size of $\frac{\lambda}{7}$ could be discerned by isopropyl alcohol (IPA)-immersed BTG microspheres with diameters of 4.2 μm. Following this work, a great deal of effort has been devoted to analyzing the influences of the different refractive indices of immersion liquid and microspheres, as well as the influence of the height of the immersion liquid on the imaging properties [54,69,88–91]. Thus far, the reported minimum feature discerned by liquid-immersed microspheres is a 25-nm gap between a pair of nanodots, as shown in Fig. 4(b) [34]. Liquid-immersed microspheres have been demonstrated to be highly advantageous for biological applications, which will be discussed in detail later.

Aside from immersing microspheres in liquid, Darafsheh et al. [78] demonstrated that high-refractive-index microspheres embedded in transparent solid films can achieve super-resolution imaging. Typical fabrication processes of embedding BTG microspheres in a PDMS film are illustrated in Fig. 4(c) [68]. In the experiments, 30–150 μm BTG microspheres were embedded in a PDMS

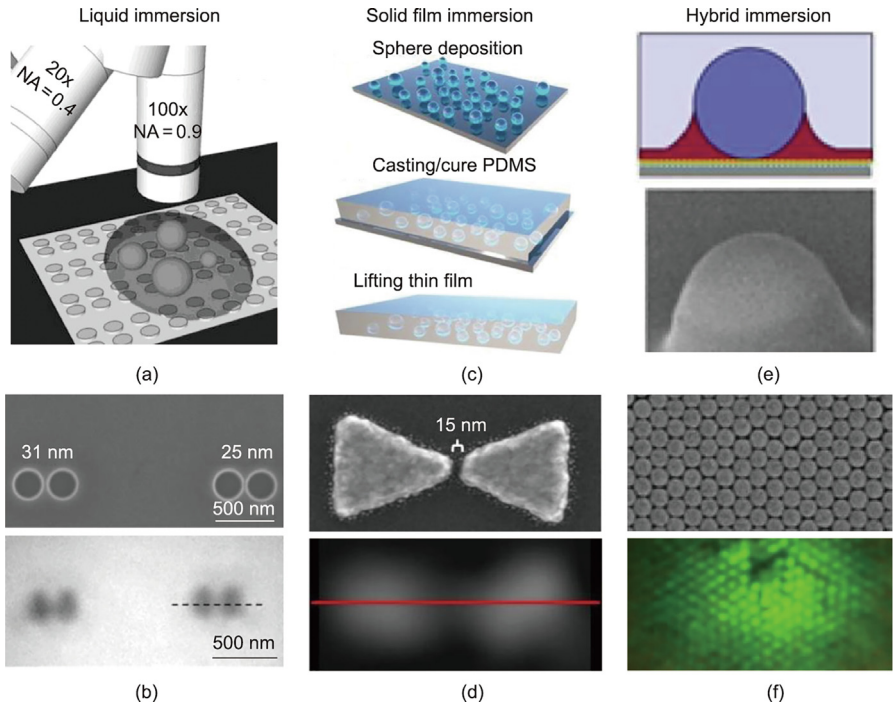

Fig. 4. (a, c, e) Schematics of microsphere nanoscopes working in (a) liquid-immersion, (c) solid-film-immersion and (e) hybrid-film-immersion environments. (b, d, f) Microscopy images of (b) separated nano-dots captured by microspheres in a liquid immersion environment, (d) a bowtie pattern obtained by BTG microspheres immersed in a PDMS film, and (f) a 200 nm-diameter silica nanosphere array observed through BTG microspheres immersed in a photoresist-PDMS hybrid film. The upper parts of the images in (b), (d), and (f) are the scanning electron microscope (SEM) images of samples. Part (a) reproduced from Ref. [87] with permission; (b) reproduced from Ref. [34] with permission; (c) and (d) reproduced from Ref. [68] with permission; (e) and (f) reproduced from Ref. [92] with permission.

elastomer, which enhanced the imaging resolution by a factor of two. Compared with liquid-immersion schemes, the PDMS membrane can be prefabricated for biological applications and is not susceptible to the effects of evaporation. Du et al. [93] analyzed the effect of film thickness on the imaging properties of microspheres and found that the FOV of the microsphere increases with a reduction in the film thickness. Furthermore, when high-refractive-index microspheres are partially immersed in SU-8 photoresist, the imaging distortion can be significantly reduced [94]. In 2018, Wang et al. [92] proposed a more complicated immersion scheme with a hybrid film structure. As shown in Fig. 4(e), the half body of a BTG microsphere is immersed in an S1805 layer, and the residual part is immersed in PDMS with a refractive index of 1.4. Due to the increased NA, this configuration can resolve a 200 nm silica microsphere array, as shown in Fig. 4(f), whereas a BTG microsphere fully immersed in PDMS or liquid cannot even discern a 250 nm silica microsphere array. Embedding microspheres in PDMS thin films can simultaneously improve the imaging resolution and assist in manipulating the motion of the microspheres, as mentioned earlier. By using microspheres embedded in thin films to scan samples, high-resolution images of a large area can be achieved, greatly promoting imaging efficiency [68,85].

2.6. Integrating microspheres with other microscopy techniques

The microsphere lens is a versatile nano-imaging device that can be integrated with various advanced microscopy platforms to achieve enhanced nano-imaging by leveraging the strengths of both techniques. The combination of microspheres with other microscopy techniques is straightforward, owing to the microscale geometry and virtual imaging principle of microspheres. According to the virtual imaging principle, the microsphere produces a virtual image of a sample, which can be taken as the new imaging target of the paired microscope. Since the enlarged virtual image produced by a microsphere inherently contains the information of features with a size beyond the optical diffraction limit, the microscope integrated with the microsphere exhibits better performance compared with its independent function.

In 2013, Yan et al. [67] made the initial effort to integrate a microsphere with a confocal microscope. As shown in Fig. 5(a), the researchers placed a fused silica microsphere on an AAO sample and used a conventional confocal laser scanning microscope to capture the virtual image produced by the microsphere. Taking advantage of the high signal-to-noise ratio of the confocal laser scanning microscope and the virtual imaging magnification ability of the microsphere, they discerned holes in an AAO template with sizes as small as 25 nm, as displayed in Fig. 5(d), which was significantly superior to the independent performance of a conventional confocal laser scanning microscope. Inspired by the function of pinholes in a confocal microscope, Zhou et al. [95] added an aperture to a conventional bright-field microsphere nanoscope, as shown in Fig. 5(b), and achieved greater imaging contrast than with the original configuration. The researchers referred to this setup as a "confocal optical microsphere imaging microscope." Since the microsphere is attached to a holder, this setup is also capable of acquiring 3D images of samples by scanning. A typical 3D imaging result is presented in Fig. 5(e). Compared with a commercial confocal laser-scanning microscope, its 3D scanning imaging speed is about nine times faster, since it works in an image-by-image scanning manner.

Microspheres have also been successfully integrated with a dark-field microscope, optical endoscope, and optical interference microscope [96–98]. Zhou et al. [99] experimentally demonstrated that the imaging contrast and uniformity can be greatly improved when a microsphere is combined with a dark-field microscope. The imaging resolutions of current endoscopes are usually confined to about 1 μm. By attaching a microsphere to the detection end of a gradient-index (GRIN) lens-based endoscope probe, the endoscope

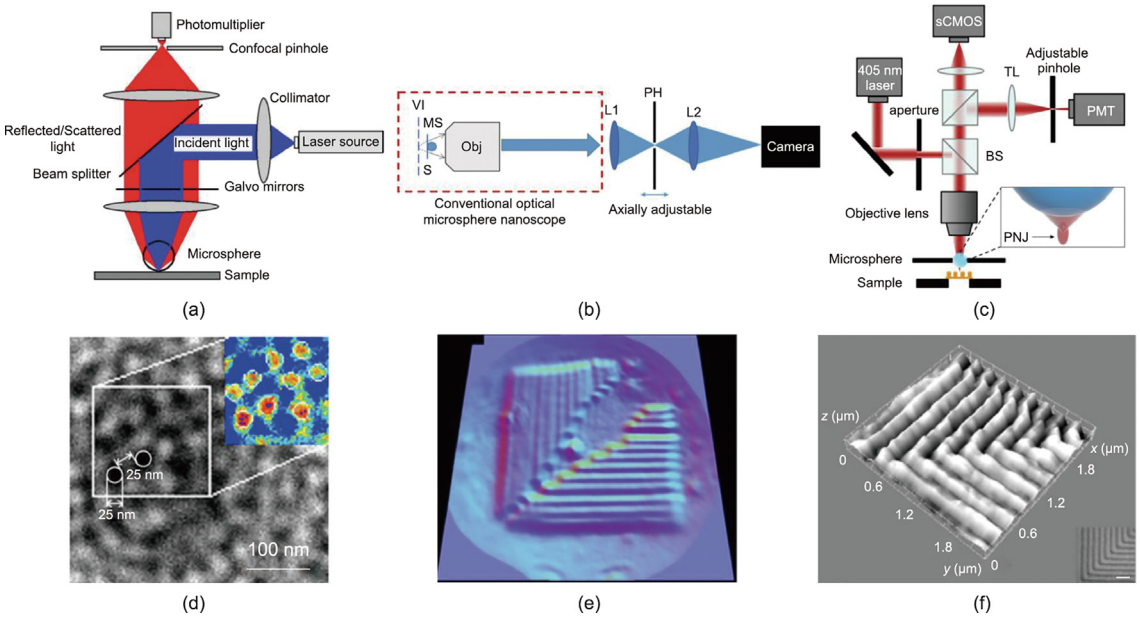

Fig. 5. Integrating microspheres with confocal microscopes. (a) A microsphere deposited on the sample surface for virtual imaging; (b) a microsphere controlled by a holder for virtual imaging. VI: virtual image plane; MS: microsphere; S: sample plane; L1 and L2: focusing lenses; Obj: objective lens; PH: pinhole; (c) a microsphere controlled by a holder for light-focusing scanning imaging. sCOMS: scientific complementary metal-oxide-semiconductor; PMT: photomultiplier tube; BS: beam splitter; PNJ: photonic nanojet; TL: tube lens; (d–f) Imaging results captured by the microscopes in (a–c), respectively. Parts (a) and (d) reproduced from Ref. [67] with permission; (b) and (e) reproduced from Ref. [95] with permission; (c) and (f) reproduced from Ref. [60] with permission.

can resolve objects with a feature size of about $\frac{\lambda}{5}$, which significantly outstrips the resolution of conventional GRIN lens-based endoscopes and breaks the optical diffraction barrier [100].

Many other reported works have combined microsphere nano-imaging techniques with an interferometry microscope to enhance the 3D imaging resolution [97,101]. Wang et al. [102] reported a microsphere-assisted white-light interferometry system, which was modified from white-light interferometry with a Linnik configuration by inserting a microsphere into the object arm. Exploiting the high axial topography profiling resolution of the white-light interferometer and the outstanding lateral resolution of the microsphere, this system can resolve features with a minimum size of about 50 nm and about 10 nm in the lateral and axial dimensions, respectively. This system can also function in both air and liquid environments, exhibiting remarkable versatility. Aakhte et al. [103] integrated a microsphere with a low-magnification Mirau interferometric objective in a common-path digital holographic microscope to achieve a high NA at a relatively low cost. Later, Kassamakov et al. [104] employed a similar system and achieved a lateral resolution of 112 nm, increasing the imaging resolution by a factor of five. Their simulations revealed that the improved resolution of nano-imaging is largely attributed to the phase change of the reflected wave. Subsequently, a phase-shifting interference microscope was integrated with a microsphere by Perrin et al. [101] and Leong-Hoi et al. [105]. The lateral resolution was enhanced by a factor of about 4, while the axial sensitivity was maintained at several nanometers with a low-NA (~0.3) objective lens. Nevertheless, the incorporation of a single microsphere in the object arm can result in significant spherical aberrations due to the asymmetrical interferometer configuration. Perrin et al. [106] later solved this problem by integrating two microspheres in both the object and reference arms. This straightforward modification significantly improves the spatial resolution.

Microspheres not only possess extraordinary resolving power in virtual imaging but also have a strong light-focusing ability, which is well known as the photonic nanojet effect. Therefore, it is also of great interest to integrate microspheres with various microscopy techniques by utilizing their exceptional focusing ability. Yang et al. [60] modified a commercial confocal microscope with an adjustable pinhole and successfully exploited a microsphere as its focal lens for resolution-enhanced scanning imaging, as shown in Figs. 5(c) and (f). This microsphere-assisted confocal microscope achieved an axial resolution of 100 nm and provided 4.56 times better image contrast because the microsphere simultaneously reduced the focusing spot and promoted the collection efficiency of scattered light. Due to their enhanced light excitation and collection ability, microspheres also have great application potential when integrated with fluorescence-based microscopy techniques and optical fiber probes [107–110]. For example, Yang et al. [108] fabricated an array of dielectric microspheres and utilized photonic nanojets to detect fluorescent nanoparticles. Their experiments demonstrated that fluorescent nanoparticles with a diameter as small as 20 nm could be detected, and the fluorescence intensity was enhanced by approximately 40 times.

2.7. Nano-imaging applications

Over the past few decades, significant progress has been made in improving the imaging performance of microsphere nanoscopes, as discussed above. In particular, the locomotion of the microsphere has greatly enhanced the versatility of this technology, reducing the gap between laboratory prototypes and industrial requirements. In 2021, the startup company Phaos Technology Pte. Ltd. (Singapore) successfully brought out their first-generation microsphere nanoscope (OptoNano 200), which can achieve 137 nm imaging resolution in ambient air. Another company, LIG-Nanowise (United Kingdom), has also launched a microsphere nanoscope product, named NANORO M. The NANORO M can resolve lateral features below 100 nm, depending on the sample, with the option of using a super-resolution microsphere amplifying lens (SMAL) [112]. Xianna Precision Instruments Co. Ltd. (China) have developed a microspherical lens assembly, which can simultaneously achieve super-resolution and a super-wide FOV in air [113]. There is no doubt that, with the application of

more reported modification schemes, the commercially available microsphere nanoscope will exhibit even better imaging performance.

So far, many application scenarios of the microsphere nanoscope have been explored, according to its imaging characteristics. The most potential and valuable application would be in the semiconductor industry. With the development of semiconductor fabrication, the sizes of metal wires and functional devices in a semiconductor chip have decreased far beyond the optical diffraction limit. Given its cost-effectiveness and label-free nature, the microsphere nano-imaging technique is an attractive option for semiconductor inspection during fabrication and quality checks. Using a microsphere nanoscope equipped with a holder, any position of interest on a semiconductor chip can be observed. Furthermore, an image of a large area of the semiconductor chip can be acquired via scanning and image stitching. A typical image of an industrial semiconductor product captured by a BTG microsphere is presented in Fig. 6(a), which shows the magnetic head in a hard disc drive with a minimum feature size of 77 nm [34].

In addition to imaging the surface pattern, microsphere nanoscopes are capable of sub-surface nano-imaging, which is a unique advantage compared with scanning electronic microscopy and standard scanning probe microscopy [114]. For example, Lee et al. [114] and Guo et al. [115] used a microsphere nanoscope to directly observe sub-surface Blu-ray recorded data structures (100–200 nm), which are outside the resolution limit of conventional optical microscopes. Furthermore, a microsphere-assisted interference microscope can reconstruct the 3D surface of nanostructures, as has been demonstrated in diverse samples, including silicon gratings, periodic Ag nano-dots on silicon, and periodic ripples in stainless steel [102,105,106]. It should be noted that the microsphere nanoscope excels in plasmonic interaction imaging for samples with special metal nanostructures. The surface plasmonic resonance effect can enhance the imaging resolution of the microsphere nanoscope, which is supported by many application examples presented in Section 2.1.

The biological field is another important application direction of the microsphere nano-imaging technique, which exhibits three advantages in this field. First, the microsphere can function in both air and liquid environments, allowing live biological samples in liquid to be observed. Second, since the microsphere nanoscope does not necessitate the use of fluorescent labeling for imaging, it can be applied to a wide range of biological samples, whether they require labeling or are label-free. In particular, the physicochemical properties of biological samples can sometimes be altered by labeling, such that images obtained with fluorescent microscopes may not accurately reflect the original state of the sample, rendering them unreliable for subsequent studies. In this scenario, the microsphere nano-imaging technique can be an indispensable alternative for the frequently used fluorescent super-resolution microscopes. Third, the microsphere nanoscope is capable of monitoring the activities of biological samples in real time and does not require image reconstruction.

To validate the effectiveness of the microsphere nano-imaging technique for biological applications, microspheres were applied to image diverse biological specimens. Li et al. [116] successfully observed 75 nm adenoviruses using a submerged microsphere nanoscope without fluorescent labeling. Yang et al. [27] observed diverse fluorescent samples—including fluorescent particles, subcellular structures in AML12 cells, and MTCO1 proteins—using a liquid-immersed high-refractive-index microsphere. Fig. 6(b) displays the imaging results of mitochondria in AML12 cells captured by both conventional fluorescent microscopy and a microsphere nanoscope. More details of the cells can be discerned in the image captured by a single microsphere. In their experiment, samples with a minimum size of about $\frac{\lambda}{7}$ were discerned. Li et al. [57] and Gao et al. [117] reported enhanced imaging results of human epithelial cells and rat liver slices using microspheres. Microsphere nanoscopes can also be used for the sub-diffraction-limited color imaging of nano biostructures. The color properties of biostructures cannot be extracted by other analytical tools, such as scanning electron microscopy and transmission electron microscopy, whereas the microsphere nanoscope captures color effectively. For example, Jia et al. [118] successfully resolved the nanoscale features of butterfly wing scales with their real color property using microspherical superlenses. These features have never been resolved by conventional optical microscopes.

Quantum dots are excellent fluorescent tags for labeling biological samples. The microsphere nanoscope has also been demonstrated to be effective in applications of quantum dot luminescence collection enhancement. For example, Zhang et al. [119] demonstrated that the presence of microspheres enabled a conventional optical microscope to observe the “blinking” phenomenon of quantum dots under a low-magnification and low-NA objective. They attributed the luminescence collection enhancement to three aspects: First, the quantum dots excitation is intensified due to focused illumination light. Second, the microsphere provides a larger NA to collect the light rays. Third, the

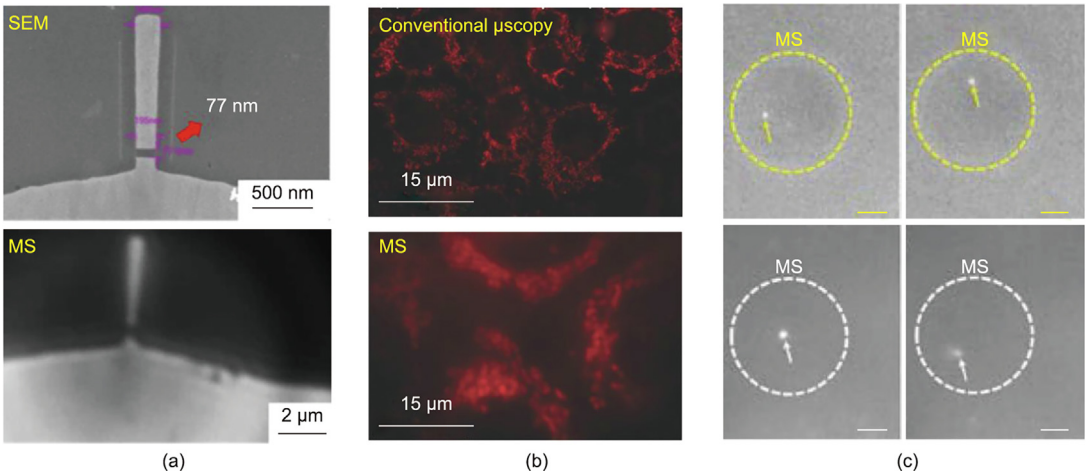

Fig. 6. (a) Images of a magnetic head with a 77 nm minimum feature size in a hard disc drive obtained via SEM and a microsphere nanoscope (MS). (b) Fluorescent microscopy images of mitochondria captured by a conventional fluorescent microscope (Conventional μscopy) and a microsphere nanoscope (MS). (c) Brownian motion of 300 nm nanoparticles in ultrapure water, recorded by a microsphere nanoscope. Parts (a), (b), and (c) reproduced from Refs. [27,34,111] with permission, respectively.

magnification of the microsphere improves the imaging resolution, considering the limited pixel size of the camera.

Recently, attempts have been made to merge microfluidics devices with microsphere nano-imaging techniques, which can be another paradigm for biological applications [120]. By embedding high-refractive-index microspheres in a PDMS membrane, Yang et al. [111] observed the Brownian motion of 300-nm polystyrene nanoparticles in water, as shown in Fig. 6(c). Jin et al. [121] successfully demonstrated the identification and classification of nanomaterials flowing in microfluidic channels using the real-time imaging results acquired via a microsphere. These results show the feasibility of integrating microspheres with microfluidic platforms for a variety of applications in biological and chemistry fields.

3. The microsphere compound lens for enhanced nano-imaging

In Section 2, we reviewed the development of single-microsphere nanoscope systems. Such schemes can improve imaging performance and promote the viability of microspheres in practical applications. However, some inherent limitations of the microsphere itself cannot be surmounted. For example, the imaging resolution of a microsphere depends on its size. As the size of the microsphere decreases, the imaging resolution becomes better, but the imaging FOV is significantly restricted. It is difficult to solve this size-induced imaging performance dilemma in a single-microsphere nano-imaging system. As the Nobel Prize winner in physics, Philip W. Anderson, has famously stated, "more is different" [122]. Compound lenses made of multiple microspheres and common lenses may also provide some unusual imaging capacities, which could potentially address certain issues present in single-microsphere nano-imaging systems. In this section, we introduce advances in constructing MCLs and using them to solve the restrictions in single-microsphere nano-imaging systems. According to the different elements employed to form the MCL, it is categorized into three types: (1) compound lenses formed by two microspheres, (2) compound lenses containing nanosphere components, and (3) compound lenses consisting of microspheres and common lenses.

3.1. Compound lenses formed by two microspheres

Macroscopical imaging devices, such as objective lenses, are generally composed of numerous well-designed lenses, which enable the devices to meet a range of imaging demands that a single lens is incapable of [123,124]. The compound lens scheme is powerful, reliable, versatile, and cost effective in practical applications. The design philosophy of macroscopic compound lenses can provide valuable guidance for upgrading microsphere nanoscopes—that is, replacing the single microsphere with an MCL. The simplest MCL is made of two vertically stacked microspheres, which involve a two-cascaded magnification process for nano-imaging. First, the primary microsphere adjacent to the sample surface produces an enlarged image of the sample, which is subsequently taken as the imaging target of the secondary microsphere and is further magnified by it. The enlarged image of the sample, with a feature size beyond the optical diffraction limit, can then be captured and resolved by means of a low-magnification objective lens in a conventional optical microscope. A single microsphere can achieve super-resolution in either virtual or real imaging modes [125]. Thus, a two-microsphere assembled MCL can work in four different combinations of imaging modes, as seen in Fig. 7(a). Different imaging modes may exhibit different imaging performances, even though they have the same cascaded magnification. The light exiting from MCLs working in different imaging modes has varied exiting angles, which subsequently affects the light collection efficiency of the objective lens and thus impacts the imaging performance. Generally speaking, the virtual-real imaging mode is preferred, owing to its large light energy collection angle and extensive operation space between the MCL and the objective lens [74].

In the quantitative design of MCLs, cascaded Gaussian imaging formulas based on geometric optics theory are utilized to determine the parameters of the microspheres, enabling the MCLs to achieve targeted imaging properties, including magnification and imaging modes. However, the imaging properties of the microspheres or MCL directly calculated by geometric optics theory are not accurate enough and show some deviation from the experimental results, due to the significant wave optics effects of the microspheres [126]. To solve this problem, Wu et al. [74] modified the Gaussian imaging formulas with a new concept, the "effective refractive index," which involves the influences of wave optics effects. The derivation of the effective refractive index is based on the focal length of the microspheres, as obtained from full-wave simulations. When the material refractive index in the Gaussian imaging formulas is substituted with the effective refractive index, more accurate imaging properties of MCLs can be acquired, which has been demonstrated by both simulations and experiments.

The first MCL was experimentally realized based on a standard inverted optical microscope, as shown in Fig. 7(b) [127]. In this MCL, the primary microsphere is immobile on the sample surface, while the secondary microsphere can move freely, as it is attached to a cantilever holder. This MCL configuration has the same problems as a single microsphere without mobility. For example, the MCL cannot relocate to points of interest for imaging at will and may cause contamination of the imaging samples. To avoid these issues, Wu et al. [74] proposed an MCL configuration that can be moved over the sample surface freely, as shown in Fig. 7(c). The two microspheres used to assemble this MCL are respectively attached to the tips of two metal holders. By mounting the metal holders on two high-precision moving stages, the two microspheres can be assembled into a vertically stacked MCL with good mobility. This MCL exhibits advantages such as versatility in both periodic and aperiodic samples and the ability to image samples with a large area via scanning.

3.2. Summary of enhanced imaging performance

MCLs formed by two vertically stacked microspheres exhibit multiple advantages over a single microsphere in nano-imaging. First, the magnification of the MCL is customizable and greater than that of a single microsphere. In the literature, a compound lens with a magnification as high as 10× was realized by adjusting the sizes of the microspheres constituting the compound lens, which is impossible for a single microsphere [74,127]. Figs. 8(a) and (b) display the imaging results of a Blu-ray disc captured by a single 23 μm silica microsphere and by an MCL consisting of 23 μm (bottom) and 102 μm (upper) silica microspheres. It is obvious that the image (Fig. 8(b)) of a Blu-ray disc captured by the MCL is almost two times larger. The imaging magnification of such an MCL is tunable by controlling the gap between the microspheres. As shown in Fig. 8(c), when the gap between the microspheres changes from 112 to 0 μm, the magnification increases from 2.8× to 10.3×, which coincides with the predictions of the modified theory based on the effective refractive index, while the conventional Gaussian imaging formula usually overestimates the magnification.

High magnification allows the MCL to pair with a low-power objective lens for nano-imaging, which not only reduces the cost of the microsphere nanoscope but also offers more space for the

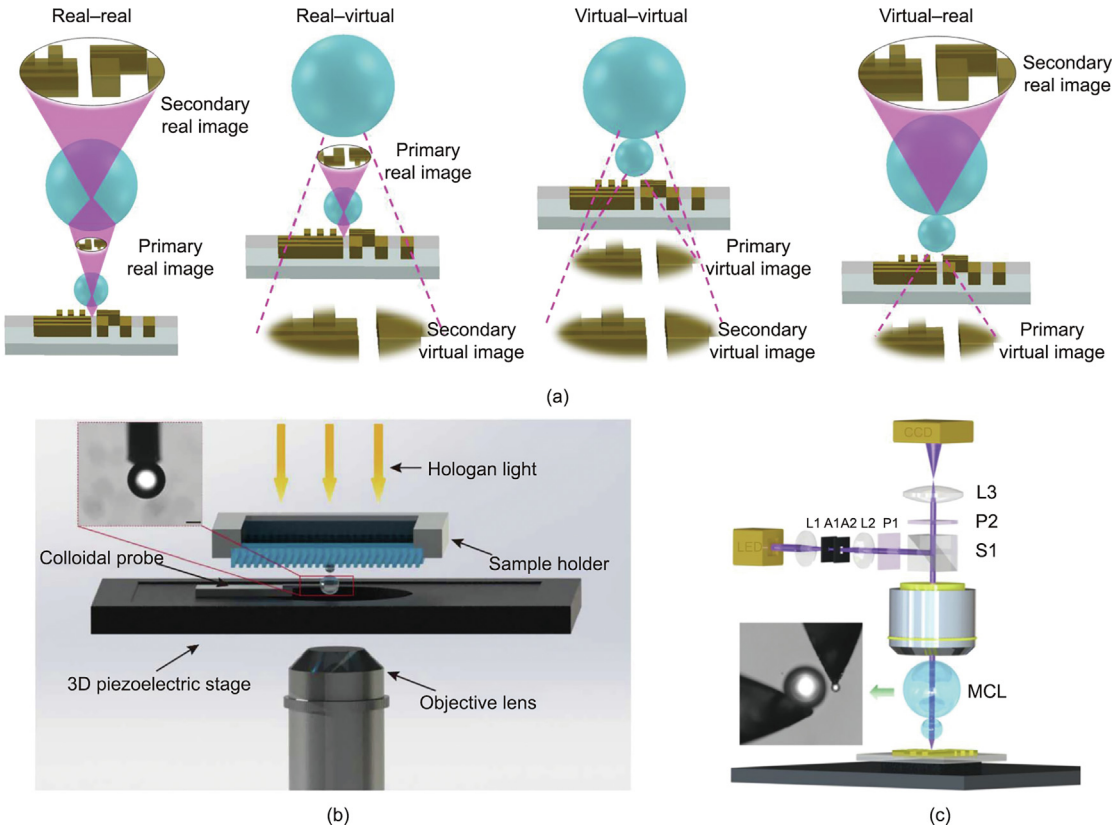

Fig. 7. (a) Schematic of the four imaging modes enabled by a compound lens consisting of two microspheres. (b) Experimental setup for an MCL without mobility. Inset: microscopy image of a microsphere in an MCL fixed on a colloidal probe. (c) Nano-imaging setup of an MCL with good mobility. Inset: A typical microscopy image of two microspheres in the MCL fixed on two separated metal tips. A1: aperture diaphragm; A2: field diaphragm; P1: polarizer; P2: analyzer; L1-L3: lens; S1: beam splitter. Parts (a) and (c) reproduced from Ref. [74] with permission; Part (b) reproduced from Ref. [127] with permission.

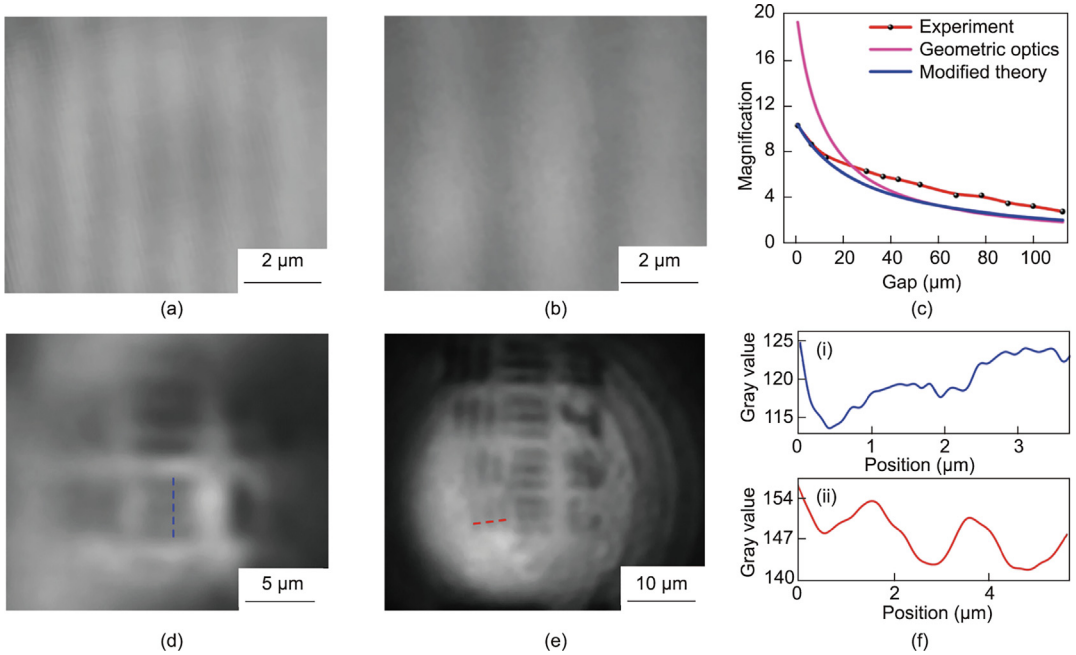

Fig. 8. Imaging magnification and FOV comparisons between single microspheres and MCLs. (a, b) A Blu-ray disc imaged by (a) a 23 μm silica microsphere and (b) an MCL formed by 23 μm and 102 μm silica microspheres. (c) Measured and calculated magnifications of the MCL vs the gap between two microspheres. (d, e) Images of a high-resolution target captured by (d) a single silica microsphere and (e) an MCL formed by 23 μm and 100 μm silica microspheres coupled with a 10× objective lens. (f) Intensity profiles along the dashed lines in (d) and (e). Reproduced from Ref. [74] with permission.

manipulation of the microspheres, due to a longer working distance. Wu et al. [74] experimentally demonstrated that a 10× objective lens (NA of ~0.3) in cooperation with an MCL could resolve a 137 nm feature size in a standard resolution target, which a single microsphere is incapable of, as compared in Figs. 8(d)–(f). In addition, it was found that the FOV of the MCL was larger than that of a single microsphere. As illustrated in Figs. 8(d) and (e), the FOV of the MCL is almost four times larger than that of a single microsphere. The larger FOV of the MCL greatly promotes the scanning speed when imaging large-area samples.

Aside from the increased magnification and FOV, Luo et al. [128] reported that a well-designed MCL can enhance the imaging contrast, compared with a single microsphere. In their experiments, the researchers used a 20 μm fused silica microsphere on the top side and a 20 μm BTG microsphere on the bottom side to construct the compound lens. An AAO sample with 100–400 nm hole features was utilized to study the imaging properties of the MCL. Imaging results captured by SEM, a fused silica microsphere in air, a BTG microsphere immersed in water, and the MCL in air are displayed in Figs. 9(a)–(d), demonstrating that the MCL achieves comparable or superior performance compared with BTG microspheres immersed in water. The improved imaging quality is ascribed to the higher contrast index of the BTG microsphere in air compared with that of the fused silica microsphere in air or the BTG microsphere in water, which enables the MCL to collect more scattered light from the sample and thus improves the overall image quality. Like the single-microsphere case, an MCL with good mobility is more versatile for practical applications. For example, it can realize nano-imaging for large-area samples via scanning. In Fig. 9(e), a five-ring pattern occupies an area beyond the FOV of the MCL, and its image cannot be obtained in a single capture. An MCL controlled by holders was utilized to scan and capture images of the pattern at eight different positions. The high-resolution image of the pattern, shown in Fig. 9(f), in which a 76 nm gap is distinguishable, was then acquired by stitching these images. The realization and demonstration of MCLs with mobility drive this technology towards practicality.

3.3. Compound lenses containing nanosphere components

As discussed earlier, the imaging resolution of microspheres increases as their sizes decrease, which raises an intriguing question about whether nanospheres can yield even better imaging resolution than microspheres. However, the FOV of a single nanosphere is too small to cover most patterns; thus, it is difficult to validate this speculation. In the compound lens paradigm, such a size barrier can be overcome by assembling multiple nanospheres into a compound lens for nano-imaging. Thus far, two kinds of compound lenses containing nanosphere components have been proposed, as displayed in Figs. 10(a) and (b). The first type (Fig. 10(a)) comprises a microsphere situated on the top side, surrounded by several nanospheres on the bottom side [129]. Experimental results have demonstrated that such an MCL can increase the imaging magnification based on a similar principle as the compound lens made up of two microspheres. Regrettably, no experimental results have been provided of resolution enhancement with such an MCL configuration.

The second type of compound lens (Fig. 10(b)) does not involve a microsphere component and completely consists of nanospheres. In 2015, Zhu et al. [130] chemically synthesized high-refractive-index nanocomposite microspheres using a nanoparticle-hybrid-suspension polymerization approach with ZrO_2 and polystyrene nanospheres as the building blocks. The refractive index of the nanocomposite microspheres could be controlled by changing the volume fractions of the ZrO_2 and polystyrene nanospheres. The researchers obtained a variety of nanocomposite microspheres with sizes ranging from 2 to 20 μm and refractive indices between 1.590 and 1.685. The imaging resolution and quality of these nanocomposite microspheres improved with an increase in their refractive indices. In particular, when a nanocomposite microsphere (n of ~1.685) was semi-immersed in cedarwood oil (n of ~1.515), 60 nm gaps in a sample could be discerned. The nanocomposite microsphere is thought to utilize a similar super-resolution mechanism as common microspheres. Later, Dhama et al. [131] employed 20 nm TiO_2 (n = 2.5) nanospheres as the basic components to synthesize nanocomposite microspheres. To directly com-

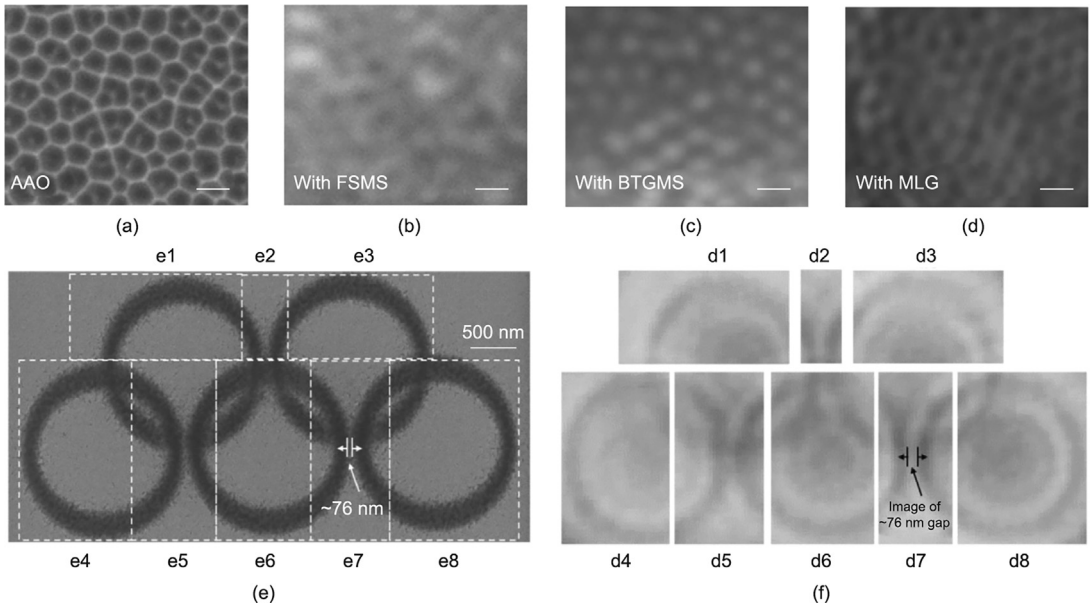

Fig. 9. (a–d) An AAO sample imaged by (a) SEM, (b) a 20 μm fused silica microsphere (FSMS) in air, (c) a 20 μm BTG microsphere (BTGMS) immersed in water, and (d) an MCL formed by a 20 μm fused silica microsphere and a 20 μm BTG microsphere in air. MLG: microsphere lens group. (The scale bar in (a–d) is 500 nm.) (e, f) Images of a five-ring pattern obtained by (e) SEM and (f) an MCL formed by 30 μm and 80 μm BTG microspheres in oil. The subfigures d1-d8 correspond to regions e1-e8 of the five-ring pattern. Parts (a–d) reproduced from Ref. [128] with permission; Parts (e–f) reproduced from Ref. [74] with permission.

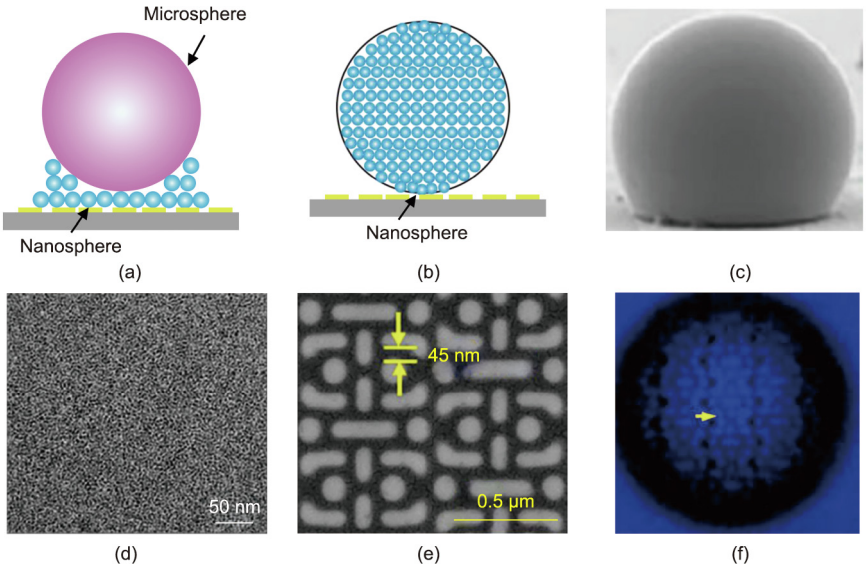

Fig. 10. (a, b) Schematic of (a) an MCL consisting of a microsphere and some nanospheres, and (b) an MCL completely consisting of nanospheres. (c) Low-magnification and (d) high-magnification SEM images of a fabricated plano-spherical microlens consisting of polymer nanospheres and modified ZrO_2 nanospheres. (e, f) Images of a chip with 45 nm features captured by (e) SEM and (f) a plano-spherical microlens. Parts (c–f) reproduced from Ref. [132] with permission.

pare the imaging performance of a BTG microsphere with that of the nanocomposite microsphere, the effective refractive index of the nanocomposite microsphere was designed to be the same as the BTG microsphere—that is, 1.92—by controlling the volume ratio of TiO_2 nanospheres. Both the BTG microsphere and the nanocomposite microsphere were embedded in a PDMS membrane for nano-imaging. The imaging results demonstrated that 90 nm line features on a wafer could only be resolved by the nanocomposite microsphere, while the BTG microsphere was incapable of doing so. The researchers suggested that 20 nm nanospheres can modulate light at a very high frequency, which enables more evanescent wave components to be converted into propagation waves and thus enhances the imaging resolution. These results show that compound lenses made of nanospheres can achieve higher imaging resolution than common microspheres.

In addition to forming MCLs with spherical geometry, nanospheres can be used to construct plano-spherical microlenses, which have been demonstrated to have superior imaging resolution in comparison with nanocomposite microspheres. In 2016, Fan et al. [133] fabricated an all-dielectric plano-spherical microlens using 15 nm TiO_2 nanospheres with a unique "nano-solid-fluid assembly" method. In the experiment, tightly packed TiO_2 nanospheres immersed in an organic solvent mixture were sprayed onto the sample surface. Due to gravity and interfacial tension, the droplets naturally deformed into a plano-spherical shape. After the evaporation of the organic solvent mixture, a plano-spherical microlens made of TiO_2 nanospheres was prepared and could be used for nano-imaging. This plano-spherical microlens could discern features with sizes of about 45 nm under white light illumination. Simulations revealed that the 15 nm TiO_2 nanospheres in the microlens could produce nanoscale light spots over large areas, aiding in the conversion of evanescent waves into propagating waves and thereby enhancing the imaging resolution. Moreover, the increased NA of the plano-spherical microlens configuration is also likely to be an important factor in the improvement of imaging resolution. Considering that the plano-spherical microlens made of TiO_2 nanospheres is easily dissolved in aqueous media, Zhu et al. [132] later assembled an organic-inorganic hybrid plano-spherical microlens. The selected organic and inorganic nanospheres were polymer nanospheres and modified ZrO_2 nanospheres (n = 2.2), respectively. An SEM image of a typical plano-spherical microlens made using this approach is displayed in Fig. 10(c). Two different nanosphere components can be observed from the high-magnification SEM image (Fig. 10(d)) of the microlens. Imaging experiments demonstrated that the microlens could resolve features of about 45 nm in a semiconductor chip under blue light illumination, as shown in Figs. 10(e) and (f).

3.4. Compound lenses consisting of microspheres and common lenses

The third type of compound lens is composed of microspheres and common lenses, such as an objective lens and a microlens. Several research groups have developed methods to integrate a single microsphere with an objective lens, as illustrated in Fig. 11(a). In a design proposed by Stanescu et al. [112], a BTG microsphere is embedded in a thin layer of ultraviolet (UV)-curable glue spin-coated on a glass disk. The BTG microsphere, UV glue, and glass disk work together as a fixed lens assembly, which is further integrated with the objective lens in a replaceable manner so that the microsphere can be easily replaced on demand. The whole compound lens is named as SMAL (super-resolution microsphere amplifying lens) objective lens, which has been made into a commercial product by LIG Nanowise company (United Kingdom). Another design proposed by Yan et al. [134] is called the superlensing microscope objective lens; it consists of a conventional objective lens, a lens adaptor printed with a 3D plastic printer, and a coverslip superlens. In the coverslip superlens, high-index microspheres are completely immersed within a transparent host material, such as polymethyl methacrylate (PMMA) or PDMS, with their bottom touching the coverslip surface. The coverslip superlens is glued on the bottom end of the adaptor, which is nested outside the objective lens. The distance between the microsphere and the objective lens can be changed by adjusting the fixing position of the adaptor. Huszka et al. [135] proposed a similar compound lens configuration, in which the adaptor is a cage metal frame. To promote the scanning speed, a microsphere array is fabricated in the coverslip.

The integration of microspheres and objective lenses brings many benefits. These compound lenses can scan and image large-area samples at will without exploiting additional microsphere holders; thus, they are cost effective for super-resolution scanning imaging. Moreover, the operational complexity of such

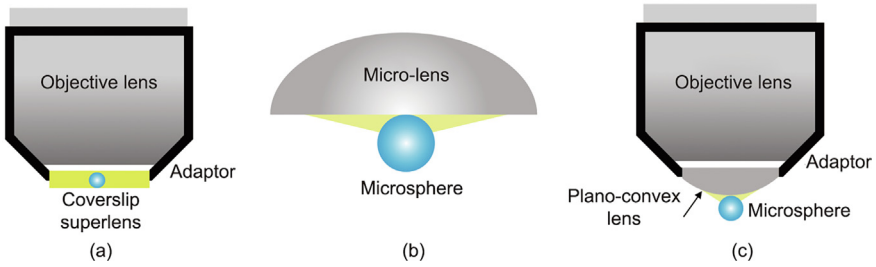

Fig. 11. Schematic of compound lenses assembled from (a) a microsphere and an objective lens, (b) a microsphere and a microlens, and (c) a microsphere, a plano-convex lens, and an objective lens.

microsphere nanoscopes is significantly reduced because only the distance between the microsphere and the objective lens requires fine-tuning. Users can utilize the microsphere nanoscope without special training, which facilitates its commercialization.

In addition to integration with objective lenses, efforts have also been made to assemble microspheres and micro-lenses into compound lenses. In 2020, Suzhou Xianna Precision Instruments Co. Ltd. (China) invented a compound lens made of a BTG microsphere and a microspherical crown lens [113]. The BTG microsphere is glued at the bottom flat surface of the micro-lens using optical adhesive, as illustrated in Fig. 11(b). When the size of the BTG microsphere and the curvature of the microspherical crown lens are appropriately selected, the compound lens can simultaneously achieve super-resolution and a super-wide FOV in air, which is superior to the single microsphere nano-imaging scheme. In the same year, Yan et al. [136] proposed another compound lens design called the plano-convex-microsphere (PCM) objective lens. The PCM objective lens consists of a BTG microsphere, a plano-convex lens, and an objective lens, as illustrated in Fig. 11(c). The BTG microsphere is partially submerged in the PDMS film that is pre-coated on the curved surface of the plano-convex lens. The whole lens assembly is integrated with the objective lens through a custom-designed objective adaptor. The PCM objective lens has been demonstrated to achieve a $\lambda/3$ calibrated resolution at a working distance of 3.5 μm, which makes this compound lens appealing for commercialization.

As discussed earlier, synergetic combinations of microspheres, nanospheres, and common lenses lead to a variety of light modulation possibilities, giving great promise to the unprecedented functionality of the compound lens. To date, diverse MCLs have yielded imaging performance enhancement in many aspects, including magnification, FOV, image contrast, and imaging resolution. Therefore, the research on MCLs remains highly relevant and deserves concentrated effort.

4. Engineered microspheres for enhanced nano-imaging

In this section, an overview of the advancements in utilizing engineered microspheres to promote microsphere nano-imaging performance is summarized. Engineered microspheres, as the name implies, are microspheres that have been tailored in terms of their shape, surface, or material. Approaches to modify individual microspheres can be categorized into three types. The first approach is to change the geometry of the microsphere or create certain micro/nano-structures in the microsphere by removing some material. These approaches can be called "subtractive manufacturing schemes". The second approach is to add other materials to the surface of the microsphere to form a special shape or structure, in what can be called "additive manufacturing schemes". The third approach involves the use of high temperature and pressure to alter the geometry of the microsphere in order to regulate the light field propagation. Engineered microspheres exhibit significantly different light manipulation and propagation properties, which can help to solve specific imaging problems presented by common microspheres. Here, two types of engineered microspheres with different enhanced functionalities realized by the three fabrication schemes are presented in detail: the plano-spherical microlens (PSML) to enhance imaging resolution and film-decorated microspheres to improve imaging contrast. In addition, some other modalities of engineered microspheres, which have not been used in imaging applications but may inspire researchers in this field, are briefly introduced.

4.1. Plano-spherical microlenses to enhance imaging resolution

The practical imaging resolution of an optical microsphere nanoscope is significantly influenced by the magnification and the NA of the microsphere. When the size of an object is beyond the optical diffraction limit, a high magnification is necessary for the microsphere to generate a large enough image of the object so that the subsequent conventional objective lens can resolve it. Furthermore, the NA of the microsphere restricts the spatial frequency bandwidth of light that can be received and transformed by the microsphere and is thus the dominant influence on the imaging resolution, as has been demonstrated in the dielectric immersed microspheres mentioned in Section 2.5. Therefore, approaches to increase the magnification and NA of microspheres are important avenues for imaging resolution enhancement and require exploration.

In Section 3, we elaborated that the PSML formed by multiple nanospheres exhibits outstanding imaging capacities. Unlike microspheres, the PSML provides the flexibility to achieve the desired magnification and NA by adjusting its lens thickness-to-diameter ratio. Therefore, the PSML can be a competent technique to circumvent the magnification and NA restrictions in microspheres and upgrade the nano-imaging resolution. To date, many engineering methods for fabricating PSMLs have been proposed, in addition to the compound lens approach presented in Section 3. In 2009, Lee et al. [140] were the first to demonstrate that a PSML created via the self-assembly of calix hydroquinone molecules could achieve an imaging resolution beyond the optical diffraction limit. Numerous PSMLs with diameters up to 3 μm and varying ratios of lens thickness to diameter were fabricated. However, due to their relatively low refractive index (~1.5), the obtained PSMLs had limited magnification capability (~1.6×) in nano-imaging, which affected their potential improvement in imaging resolution. Later, Vlad et al. [137] obtained a PSML with a higher magnification using the thermal reshaping method. The effects of the annealing temperature, annealing time, and size of the original colloidal polymer microspheres on the final shape of the PSML were systematically studied, enabling the precise control of the thickness and magnification of the PSML. Figs. 12(a) and (b) displays a representative PSML fabricated via this thermal reshaping method along with the image of a hexagonal grid captured by

the PSML. The highest magnification of the PSMLs obtained by this method is approximately 3.2×. Recently, laser processing methods have also been applied to fabricate PSMLs using photosensitized materials [141]. For example, Du et al. [138] used direct laser writing lithography to manufacture wavelength-scale lenses with complex shapes for nano-imaging. The fundamental concept involves using a high-intensity laser to induce two-photon polymerization in the negative photoresist IP-Dip. Upon rinsing with the developer, the microlens-shaped polymerized photoresist remains, while the unpolymerized photoresist is removed. This 3D laser-printing technology exhibits great fabrication flexibility because it can be used to manufacture not only PSML but also microlenses with more complicated shapes, as shown in Fig. 12(c). The PSML obtained by this method can resolve features as small as 100 nm with a light wavelength of 600 nm, as displayed in Fig. 12(d). Methods for the direct transfer of polymer or nanoparticle droplets to make shape-controllable PSMLs have also been reported [142,143].

These research works greatly enrich the topic of using PSML for nano-imaging. However, the proposed approaches still have some individual drawbacks. Specifically, chemical growth, laser processing, and thermal reshaping are restricted to certain special polymer materials, which typically have low refractive indices and thus impede the promotion of NA. In addition, as the refractive indices of these PSMLs are below 2, it is impossible to achieve a PSML with a magnification factor greater than that of a microsphere without being truncated when it comes into contact with the sample surface for imaging. Therefore, the PSMLs realized by these methods typically cannot increase the NA too much and have a low magnification factor. To fully leverage the imaging potential of the PSML technique, it is vital to employ PSMLs made of materials with a refractive index greater than 2.

Recently, Wu et al. [139] put forward a top-down approach to fabricate a high-refractive-index PSML by means of the focused ion beam (FIB) milling of a microsphere. In this fabrication, high-refractive-index microspheres are fixed in the holes of a transmission electron microscope (TEM) grid. Subsequently, the material of the microspheres is removed layer by layer through the FIB setup with nanoscale accuracy. This method is versatile, as it can be applied to microspheres made of any material and thus promises great potential to make PSMLs with unprecedented imaging capacity. Fig. 12(e) displays the SEM image of a typical PSML made from a BTG microsphere (n of ~2.34) using this method, which shows that the obtained PSML has a smooth surface. Imaging experiments have demonstrated that PSMLs with 10× magnification and an NA of approximately 2.34 were realized by accurately controlling the etched height. Such PSMLs can resolve sub-50-nm features in air while paired with only a 10× objective lens, as displayed in Figs. 12 (f) and (h). In comparison with a liquid-immersed BTG microsphere, the PSML also produces higher image fidelity and contrast, which are evident in the images presented in Figs. 12(g) and (h). Wu et al. [139] also demonstrated that the engineered microsphere scheme and the MCL scheme can synergistically cooperate to achieve comprehensive imaging performance improvement. For example, if the PSML is taken as the building block to compose a compound lens, the obtained lens possesses both the high resolution of the PSML and the large FOV of the compound lens. As shown in Figs. 13(b) and (e), a single PSML cannot capture the triangle-shaped pattern (Fig. 13(a)) or the NUS letters (Fig. 13(d)) in a single image due to its limited FOV. However, when a compound lens consisting of a PSML and an approximately 95 μm borosilicate glass microsphere is utilized to image the two patterns, both patterns can be captured in a single image, and all the sub-50 nm features in the two patterns can be resolved, as shown in Figs. 13(c) and (f). These results demonstrate the great potential of merging these two techniques for enhanced nano-imaging.

4.2. Film-decorated microspheres to improve imaging contrast

Dielectric thin films are commonly applied to optical elements, such as lenses, mirrors, and prisms, in traditional optical systems to improve their performance in terms of chromatic aberration, transmittance, and reflectivity. Microsphere as a unique microscale optical lens is not perfect and has some intrinsic flaws in imaging, which can also be tackled with the modification of optical films. At present, a widely known problem in microsphere nano-imaging is the inferior imaging contrast, which significantly degrades the overall image quality. Thus far, many approaches have been proposed to improve the imaging contrast in microsphere nano-

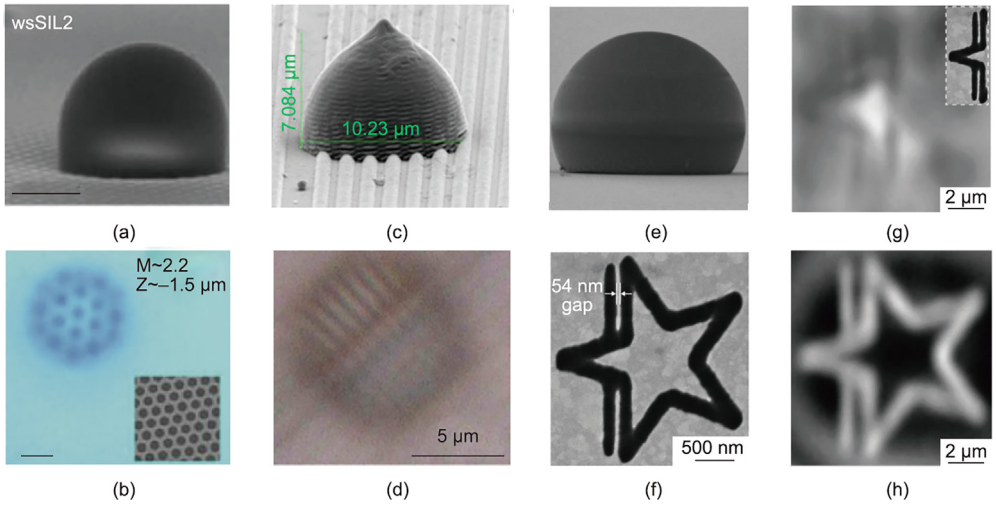

Fig. 12. (a) SEM image of a PSML fabricated via the thermal reshaping of a colloidal particle. (b) Image of a hexagonal grid with 180 nm holes and a 330 nm period acquired by the PSML presented in (a). (Scale bars in (a) and (b) represent 1 μm.) (c) SEM image of a microlens fabricated via two-photon polymerization. (d) Image of a Blu-ray disc captured by a PSML fabricated via two-photon polymerization. (e) SEM image of a PSML fabricated via focused ion beam (FIB) milling of a high-refractive-index BTG microsphere. (f–h) A star pattern with a 54 nm gap imaged by (f) SEM, (g) an 8 μm BTG microsphere (n of ~2.2) immersed in oil (n of ~1.5) and (h) a PSML fabricated via FIB milling. Parts (a) and (b) reproduced from Ref. [137] with permission; Parts (c) and (d) reproduced from Ref. [138] with permission; Parts (e–h) reproduced from Ref. [139] with permission.

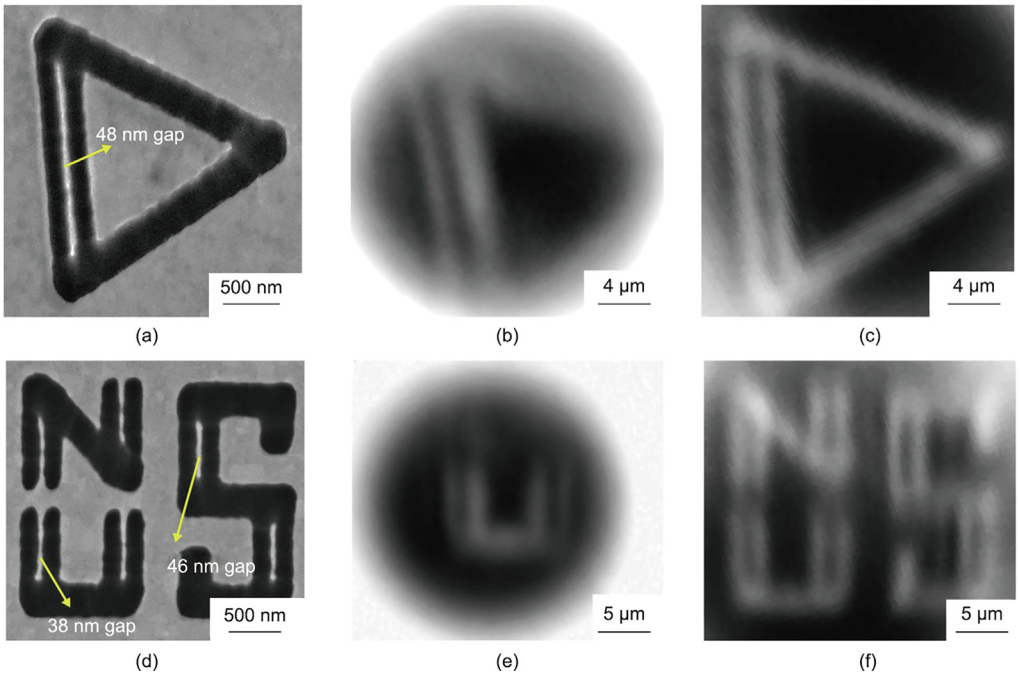

Fig. 13. Images of a triangular pattern and the letters "NUS" captured by (a, d) SEM, (b, e) a single PSML, and (c, f) a compound lens consisting of a PSML and a ~95 μm borosilicate glass microsphere. The minimum feature sizes in the triangular pattern and the "NUS" letters are 48 and 38 nm, respectively. Reproduced from Ref. [139] with permission.

imaging. Early studies were dedicated to reducing the environmental noise through the refinement of the microsphere nanoscope system. Measures such as liquid immersion, a modified illumination light source, and an optimized condenser/field diaphragm have been demonstrated to be effective in minimizing the environmental noise and thereby improving the imaging contrast. Recently, another type of engineered microsphere—that is, film-decorated microspheres fabricated via additive manufacturing schemes—has been proposed to improve the imaging contrast at the lens level.

Two strategies have been put forward to modify microspheres with thin films, as illustrated in Figs. 14(a) and (b). One strategy (Fig. 14(a)) is to use a bilayer dielectric film as the anti-reflection coating to reduce the interface reflection of the microspheres, which often leads to the appearance of Newton's rings in virtual images and thus deteriorates the imaging contrast [37,45,125]. In a physical model to reveal the formation of Newton's rings in virtual imaging, only the reflection from the bottom hemispherical surface was found to facilitate the generation of Newton's rings, while the effect of the upper hemispherical surface was negligible. The imaging simulations verified that a bilayer thin film consisting of 70 nm Al_2O_3 and 92 nm SiO_2 decorated on the bottom surface of a microsphere is sufficient to diminish the Newton's rings in virtual imaging, which was later confirmed via experiments. In the experiments, BTG microspheres were partially embedded in a PDMS membrane, and a thin film were deposited on the part that was out of the PDMS membrane. This fabrication method can ensure that the decorated area is facing the sample surface for imaging. Imaging results of a Blu-ray disc captured by a common microsphere and a bilayer-dielectric-film-decorated microsphere are shown in Figs. 14(c) and (e), respectively. The Newton's rings in Fig. 14(e) are significantly eliminated, giving the image better contrast, which can also be intuitively observed through the intensity profile, as displayed in Figs. 14(d) and (f).

The other strategy (Fig. 14(b)) to improve the imaging contrast involves using BTG microspheres with a patchy coating layer to form a photonic hook illumination condition [144]. In the experiments, 100 nm Ag films were deposited on a part of the microspheres' surface via physical vapor deposition at a constant angle. When the deposited Ag film was located on the side of the microspheres, a fraction of the incident light was obstructed by the Ag film, resulting in oblique illumination. The imaging contrast of the patchy BTG microsphere was approximately 6.5 times higher than that of a common microsphere, which was ascribed to the formation of photonic hook illumination. However, in this work, the relative position of the Ag coatings and the sample surface is uncontrollable. When the Ag film is located at a different position on the microsphere, the generated photonic hook has a varied light field distribution, which indirectly changes the illumination conditions. Not all of the changed illumination can lead to a better imaging contrast in comparison with that of common microspheres. Therefore, more efforts are required to explore new fabrication crafts so that the obtained engineered microsphere can always function in an optimized state for practical applications.

4.3. Other modalities of engineered microspheres

Other modalities of engineered microspheres have also been proposed in the literature [145–149]. Although the functions of these engineered microspheres are not designed for super-resolution virtual/real imaging, the light-manipulation approaches adopted for these engineered microspheres may offer some inspiration for designing engineered microspheres aimed at improving imaging performance. Here, three typical representatives are briefly introduced. The SEM image of a concentric-ring-decorated microsphere is shown in Fig. 15(a) [150]. The concentric ring structures were fabricated on the surface of the microsphere using FIB milling. The desired wavefront of the light exiting from the microsphere can be obtained by optimizing the ring design on the microsphere surface. A center-covered microsphere fabricated via the additive manufacturing method is presented in Fig. 15(b) [151]. This design can selectively allow light with the desired spatial frequency to pass through the microsphere and thereby achieve the light modulation. Fig. 15(c) displays the SEM image of a negative

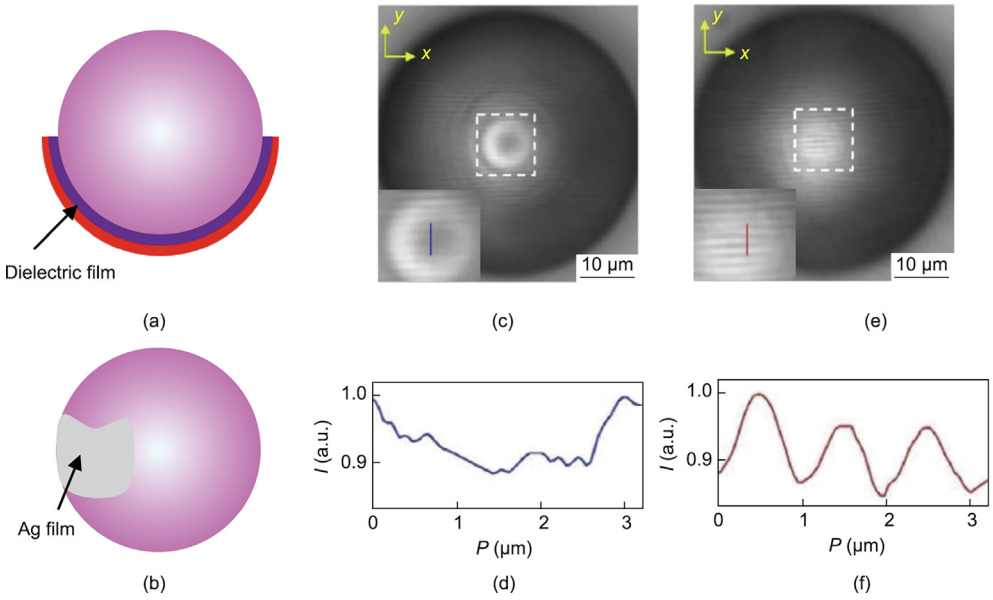

Fig. 14. (a, b) Schematic of (a) a bilayer-film-decorated microsphere and (b) a microsphere with a patchy Ag coating layer. (c, e) Images of a Blu-ray disc acquired by (c) a common 50 μm BTG microsphere and (e) a 50 μm BTG microsphere decorated with bilayer thin films. The insets in (c) and (e) are enlarged images of the area enclosed by white dashed squares. (d, f) The intensity profiles along the blue and red lines in the insets of (c) and (e), respectively. I: normalized optical intensity; P: relative position. Parts (c–f) reproduced from Ref. [37] with permission.

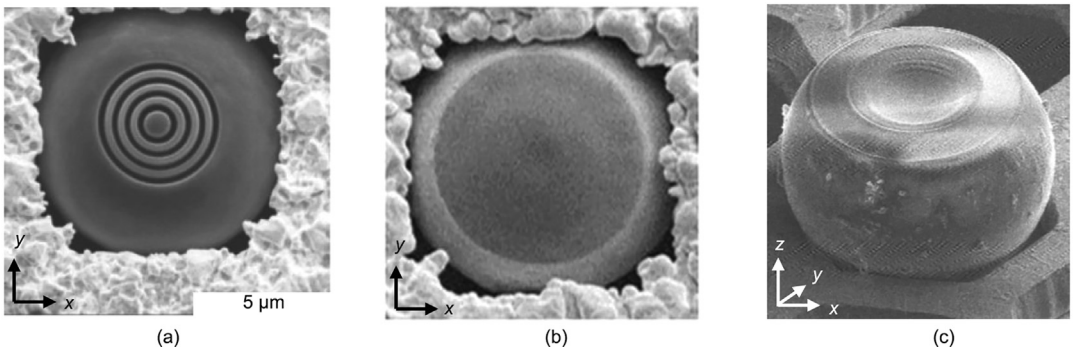

Fig. 15. SEM images of (a) a concentric ring decorated microsphere. Reproduced from Ref. [150] with permission. (b) A microsphere decorated with a platinum (Pt) mask, and (c) a negative axicon microsphere. Parts (b), and (c) reproduced from Ref. [151,152] with permission, respectively.

axicon microsphere, which was fabricated via FIB milling [152]. The negative axicon surface of this engineered microsphere can induce a path difference for light emitting at different positions so that the divergence of the emitted light becomes moderate. Unlike common microspheres, these engineered microspheres do not possess spherical symmetry. If engineered microspheres with similar modalities are designed for imaging, it will be necessary to fabricate a special holder that can move and rotate the engineered microspheres so that they can function in the correct orientation.

5. Challenges and outlooks

Although significant progress has been made in microsphere nano-imaging in recent years, this field still presents some tough challenges. Among them, the short working distance of microspheres is the most urgent issue that remains to be solved. In Section 2.4, diverse holders for supporting the locomotion of microspheres were introduced. Although the motion of microspheres in three dimensions can be well manipulated through holders, due to the limitation of the short working distance, the gap between the microspheres and the sample surfaces is restricted to several hundred nanometers or less in order to achieve high imaging resolution. The short working distance of microspheres can cause many problems in the practical usage of optical microsphere nanoscopes. First, it restricts the use of microspheres to specific surface morphology characterization applications. Applications such as observing intracellular structures with sizes beyond the optical diffraction limit or inspecting circuits inside a chip are difficult to realize using the current microsphere nanoscope. Second, the short working distance requires the sample surface to be smooth. If the sample surface is too rough, the microsphere cannot access the position of interest with a distance small enough for nano-imaging. Third, it requires precise movement stages and a control system to maintain such a short gap between the microsphere and sample surface during imaging. Otherwise, the microsphere may easily touch the sample and either the microsphere or the sample could be contaminated or even damaged. Therefore, to promote the widespread usage of microscope nano-

scopes, it is necessary to increase the working distance of microspheres via system modifications.

Aside from the fundamental working distance problem, some other problems in the microsphere nano-imaging are also yet to be solved. For example, the microsphere as a ball lens actually has severe spherical aberration and chromic aberration. It is possible to address these issues by drawing insights from the MCL and engineered microsphere techniques. In addition to the upgrade in hardware, so far, there are rarely reported works related to computational imaging in this area, which may also be effective in overcoming these challenges in microsphere nano-imaging. In particular, with rapid advances in machine learning [153,154], a state-of-art computational imaging algorithm may empower the microsphere nanoscope with unprecedented performance.

In the future, it is of great interest to fully exploit the advantages of microspheres in order to develop miniaturized and integrated optical nanoscope systems. The current microsphere nanoscope system is bulky because the microsphere must be coupled with a conventional bench-top optical microscope in nano-imaging. The conventional optical microscope in the system assists in magnifying the virtual/real images produced by the microspheres and projecting the images to the camera. With the development of the MCL technique, the conventional optical microscope in the microsphere nanoscope system is not indispensable and can be completely substituted by a well-designed compound lens, which can provide sufficient magnification and work in the real imaging mode so that the generated image of the samples can be directly projected to the camera and resolved. Therefore, it is possible to construct a compact and highly integrated optical nanoscope based on the microsphere nano-imaging technique. Such an integrated microsphere nanoscope will not only be cost effective due to its compact configuration but also possibly possess superior performance in comparison with the current bulky system. For example, the FOV of a bulky system is restricted by both the microspheres and the objective lens, which prevents the sensors in the camera from being fully used. In an integrated system, such a limitation will no longer exist. If an MCL array is directly integrated with the camera, it will be possible for the camera to be utilized to the maximum extent, while promoting the imaging throughput as well. Overall, the outstanding imaging capacity and compact geometry of microsphere lenses hold promise for a new nanoscope paradigm with a highly integrated configuration.

6. Conclusions

The optical diffraction limit is a fundamental problem in optical microscopy imaging. In the past decades, the optical microsphere nano-imaging technique has emerged as a competent technical route for overcoming this challenge. In this review, we first summarized research progress in the single microsphere nano-imaging technique. All prevailing physical models to clarify the super-resolution mechanism of microspheres were introduced and compared. Important technological evolutions that improve the microsphere nanoscope performance at the system level, including the locomotion of microspheres, dielectric medium immersion, and integration with other microscope techniques, were introduced. Then, we focused on the two most promising technological schemes—that is, MCL and engineered microspheres—which promote the imaging performance by modifying the microsphere lens itself. Diverse approaches for constructing MCLs and fabricating engineered microspheres were presented, followed by the corresponding performance enhancement in terms of magnification, resolution, contrast, FOV, and so on. Finally, we summarized the current challenges presented by microsphere nano-imaging and potential solutions. Looking forward to the forthcoming decade, we are convinced that the microsphere nanoscope can be developed toward miniaturization, with a high level of integration and good portability, which may radically revolutionize the optical nanoscopy field and have a profound influence on relevant applications.

Declaration of competing interest

The authors declare that they have no known competing financial interests or personal relationships that could have appeared to influence the work reported in this paper.

Acknowledgments

This work is supported by Innovation Laboratory for Sciences and Technologies of Energy Materials of Fujian Province Human Resource Training Project (HRTP-[2022]-53).

Compliance with ethics guidelines

Guangxing Wu and Minghui Hong declare that they have no conflict of interest or financial conflicts to disclose.

References

[1] Du E, Shen S, Qiu A, Chen N. Confocal laser speckle autocorrelation imaging of dynamic flow in microvasculature. Opto-Electron Adv 2022;5(2):210045.
[2] Zhang Y, Gross H. Systematic design of microscope objectives. Part I: system review and analysis. Adv Opt Technol 2019;8(5):313–47.
[3] Stender AS, Marchuk K, Liu C, Sander S, Meyer MW, Smith EA, et al. Single cell optical imaging and spectroscopy. Chem Rev 2013;113(4):2469–527.
[4] Abbe E. Beiträge zur Theorie des Mikroskops und der mikroskopischen Wahrnehmung. Archiv für mikroskopische Anatomie 1873;9(1):413–68. German.
[5] Lord Rayleigh FRS. XXXi. Investigations in optics, with special reference to the spectroscope. Lond Edinb Dublin Philos Mag J Sci 1879;8(49):261–74.
[6] Sparrow CM. On spectroscopic resolving power. Astrophys J 1916;44:76–86.
[7] Houston WV. A compound interferometer for fine structure work. Phys Rev 1927;29(3):478–84.
[8] Chen X. Computational methods for electromagnetic inverse scattering. Singapore: John Wiley & Sons; 2018.
[9] Fang Y, Huang Y, Liu S, Kuang C, Liu X. Superresolution optical microscopy. In: Thomas S, Thomas R, Zachariah AK, Mishra RK, editors. Microscopy methods in nanomaterials characterization. Amsterdam: Elsevier; 2017. p. 241–91.
[10] So S, Kim M, Lee D, Nguyen DM, Rho J. Overcoming diffraction limit: from microscopy to nanoscopy. Appl Spectrosc Rev 2018;53(2–4):290–312.
[11] Annibale P, Vanni S, Scarselli M, Rothlisberger U, Radenovic A. Quantitative photo activated localization microscopy: unraveling the effects of photoblinking. PLoS One 2011;6(7):e22678.
[12] Huang B, Wang W, Bates M, Zhuang X. Three-dimensional super-resolution imaging by stochastic optical reconstruction microscopy. Science 2008;319 (5864):810–3.
[13] Blom H, Widengren J. Stimulated emission depletion microscopy. Chem Rev 2017;117(11):7377–427.
[14] Rittweger E, Han KY, Irvine SE, Eggeling C, Hell SW. STED microscopy reveals crystal colour centres with nanometric resolution. Nat Photon 2009;3 (3):144–7.
[15] Weber M, Leutenegger M, Stoldt S, Jakobs S, Mihaila TS, Butkevich AN, et al. MINSTED fluorescence localization and nanoscopy. Nat Photon 2021;15 (5):361–6.
[16] Weber M, von der Emde H, Leutenegger M, Gunkel P, Sambandan S, Khan TA, et al. MINSTED nanoscopy enters the Ångström localization range. Nat Biotechnol 2023;41(4):569–76.
[17] Wang J, Zhang Z, Shen H, Wu Q, Gu M. Application and development of fluorescence probes in MINFLUX nanoscopy. J Innov Opt Health Sci 2023;16 (1):2230011.
[18] Huang K, Qin F, Liu H, Ye H, Qiu CW, Hong M, et al. Planar diffractive lenses: fundamentals, functionalities, and applications. Adv Mater 2018;30 (26):1704556.
[19] Wang Z, Luk'yanchuk B. Super-resolution imaging and microscopy by dielectric particle-lenses. In: Astratov V, editor. Label-free super-resolution microscopy. Cham: Springer; 2019. p. 371–406.
[20] Chen L, Zhou Y, Li Y, Hong M. Microsphere enhanced optical imaging and patterning: from physics to applications. Appl Phys Rev 2019;6(2):021304.
[21] Wang Z, Guo W, Li L, Luk'yanchuk B, Khan A, Liu Z, et al. Optical virtual imaging at 50 nm lateral resolution with a white-light nanoscope. Nat Commun 2011;2:218.

[22] Darafsheh A. Microsphere-assisted microscopy. J Appl Phys 2022;131 (3):031102.
[23] Li P, Li G, Yu H, Wang F, Liu L, Li WJ. Advances in dielectric microspherical lens nanoscopy: label-free superresolution imaging. IEEE Nanotechnol Mag 2021;15(1):38–51.
[24] Lukyanchuk BS, Paniagua-Domínguez R, Minin I, Minin O, Wang Z. Refractive index less than two: photonic nanojets yesterday, today and tomorrow. Opt Mater Express 2017;7(6):1820–47.
[25] Wang Z. Microsphere super-resolution imaging. In: O'Brien P, Thomas PJ, editors. Nanoscience, Vol 3. Cambridge: The Royal Society of Chemistry; 2016. p. 193–210.
[26] Brettin A, Abolmaali F, Blanchette KF, McGinnis CL, Nesmelov YE, Limberopoulos NI, et al. Enhancement of resolution in microspherical nanoscopy by coupling of fluorescent objects to plasmonic metasurfaces. Appl Phys Lett 2019;114(13):131101.
[27] Yang H, Moullan N, Auwerx J, Gijs MAM. Super-resolution biological microscopy using virtual imaging by a microsphere nanoscope. Small 2014;10(9):1712–8.
[28] Strutt HJWXV. On the light from the sky, its polarization and colour. Lond Edinb Dublin Philos Mag J Sci 1871;41(271):107–20.
[29] Bohren CF, Huffman DR. Absorption and scattering of light by small particles. New York: John Wiley & Sons; 1983.
[30] Luk'yanchuk BS, Zheng YW, Lu Y. Laser cleaning of solid surface: optical resonance and near-field effects. In: Proceedings Volume 4065, High-Power Laser Ablation III; 2000 Aug 16; Santa Fe, NM, United States. SPIE; 2000. p. 576–87.
[31] Münzer HJ, Mosbacher M, Bertsch M, Zimmermann J, Leiderer P, Boneberg J. Local field enhancement effects for nanostructuring of surfaces. J Microsc 2001;202(1):129–35.
[32] Surdo S, Duocastella M, Diaspro A. Nanopatterning with photonic nanojets: review and perspectives in biomedical research. Micromachines (Basel) 2021;12(3):256.
[33] Khan A, Wang Z, Sheikh MA, Whitehead DJ, Li L. Laser micro/nano patterning of hydrophobic surface by contact particle lens array. Appl Surf Sci 2011;258 (2):774–9.
[34] Chen L, Zhou Y, Wu M, Hong M. Remote-mode microsphere nano-imaging: new boundaries for optical microscopes. Opto-Electron Adv 2018;1 (1):170001.
[35] Yang H, Trouillon R, Huszka G, Gijs MAM. Super-resolution imaging of a dielectric microsphere is governed by the waist of its photonic nanojet. Nano Lett 2016;16(8):4862–70.
[36] Pei Y, Zang J, Yang S, Wang J, Cao Y, Ye YH. Optoplasmonic-enhanced imaging of monolayer polystyrene nanoparticle arrays by barium titanate glass microsphere-assisted microscopy: implications for nanoparticle characterization. ACS Appl Nano Mater 2021;4(10):11281–7.
[37] Wu G, Zhou Y, Hong M. Bilayer-film-decorated microsphere with suppressed interface reflection for enhanced nano-imaging. Opt Express 2022;30 (16):28279–89.
[38] Sundaram VM, Wen SB. Analysis of deep sub-micron resolution in microsphere based imaging. Appl Phys Lett 2014;105(20):204102.
[39] Heydarian R, Simovski C. Non-resonant subwavelength imaging by dielectric microparticles. Photon Nanostruct Fundam Appl 2021;46:100950.
[40] Hoang TX, Duan Y, Chen X, Barbastathis G. Focusing and imaging in microsphere-based microscopy. Opt Express 2015;23(9):12337–53.
[41] Maslov A, Astratov V. Resolution and reciprocity in microspherical nanoscopy: point-spread function versus photonic nanojets. Phys Rev Appl 2019;11(6):064004.
[42] Shi QF, Yang SL, Cao YR, Wang XQ, Chen T, Ye YH. Super-resolution imaging of low-contrast periodic nanoparticle arrays by microsphere-assisted microscopy. Chin Phys B 2021;30(4):040702.
[43] Cao Y, Wang X, Yang S, Pei Y, Zang J, Wang J, et al. Super-resolution imaging of plasmonic nanostructures by microsphere-assisted microscopy. Appl Opt 2022;61(8):E8–E13.
[44] Cao Y, Yang S, Wang J, Shi Q, Ye YH. Surface plasmon enhancement for microsphere-assisted super-resolution imaging of metallodielectric nanostructures. J Appl Phys 2020;127(23):233103.
[45] Yang S, Cao Y, Shi Q, Wang X, Chen T, Wang J, et al. Label-free super-resolution imaging of transparent dielectric objects assembled on a silver film by a microsphere-assisted microscope. J Phys Chem C 2019;123 (46):28353–8.
[46] Ben-Aryeh Y. Superresolution observed from evanescent waves transmitted through nano-corrugated metallic films. Appl Phys B 2012;109:165–70.
[47] Boudoukha R, Perrin S, Demagh A, Montgomery P, Demagh NE, Lecler S. Near-to Far-field coupling of evanescent waves by glass microspheres. Photonics 2021;8(3):73.
[48] Duan Y, Barbastathis G, Zhang B. Classical imaging theory of a microlens with super-resolution. Opt Lett 2013;38(16):2988–90.
[49] Bekirov A, Luk'yanchuk B, Fedyanin AJJL. Virtual Image within a Transparent Dielectric Sphere. JETP Lett 2020;112(6):341–5.
[50] Pahl T, Hüser L, Hagemeier S, Lehmann P. FEM-based modeling of microsphere-enhanced interferometry. Light Adv Manuf 2022;3(4):699–711.
[51] Lee S, Li L, Ben-Aryeh Y, Wang Z, Guo W. Overcoming the diffraction limit induced by microsphere optical nanoscopy. J Opt 2013;15(12):125710.
[52] Hao X, Kuang C, Liu X, Zhang H, Li Y. Microsphere based microscope with optical super-resolution capability. Appl Phys Lett 2011;99(20):203102.
[53] Ben-Aryeh Y. Increase of resolution by use of microspheres related to complex Snell's law. J Opt Soc Am A 2016;33(12):2284–8.
[54] Yang S, Ye YH, Shi Q, Zhang J. Converting evanescent waves into propagating waves: the super-resolution mechanism in microsphere-assisted microscopy. J Phys Chem C 2020;124(47):25951–6.
[55] Ye R, Ye YH, Ma HF, Ma J, Wang B, Yao J, et al. Experimental far-field imaging properties of a∼ 5-μm diameter spherical lens. Opt Lett 2013;38 (11):1829–31.
[56] Chen X, Wu T, Gong Z, Li Y, Zhang Y, Li B. Subwavelength imaging and detection using adjustable and movable droplet microlenses. Photon Res 2020;8(3):225–34.
[57] Li Y, Liu X, Li B. Single-cell biomagnifier for optical nanoscopes and nanotweezers. Light Sci Appl 2019;8:61.
[58] Zhang T, Yu H, Shi J, Wang X, Luo H, Lin D, et al. Correlative AFM and scanning microlens microscopy for time-efficient multiscale imaging. Adv Sci 2022;9 (12):2103902.
[59] Yang S, Wang F, Ye Y, Xia Y, Deng Y, Wang J, et al. Influence of the photonic nanojet of microspheres on microsphere imaging. Opt Express 2017;25 (22):27551–8.
[60] Yang X, Hong M. Enhancement of axial resolution and image contrast of a confocal microscope by a microsphere working in noncontact mode. Appl Opt 2021;60(17):5271–7.
[61] Zhou S, Deng Y, Zhou W, Yu M, Urbach H, Wu Y. Effects of whispering gallery mode in microsphere super-resolution imaging. Appl Phys B 2017;123:236.
[62] Minin IV, Minin OV, Zhou S. Influence of the environment on the effect of super resonance in mesoscale dielectric spheres. In: Zhou Z, Wada K, Tong L, editors. SPIE/COS Photonics Asia 2022: Proceedings Volume 12322, Nanophotonics, Micro/Nano Optics, and Plasmonics VIII; 2022 Dec 5–12; Online Only, China. SPIE; 2023. p. 92–9.
[63] Maslov AV, Astratov VN. Imaging of sub-wavelength structures radiating coherently near microspheres. Appl Phys Lett 2016;108(5):051104.
[64] Bekirov AR, Luk'yanchuk BS, Wang Z, Fedyanin AA. Wave theory of virtual image. Opt Mater Express 2021;11(11):3646–55.
[65] Maslov AV, Astratov VN. Optical nanoscopy with contact Mie-particles: resolution analysis. Appl Phys Lett 2017;110(26):261107.
[66] Darafsheh A, Abbasian V. Dielectric microspheres enhance microscopy resolution mainly due to increasing the effective numerical aperture. Light Sci Appl 2023;12:22.
[67] Yan Y, Li L, Feng C, Guo W, Lee S, Hong M. Microsphere-coupled scanning laser confocal nanoscope for sub-diffraction-limited imaging at 25 nm lateral resolution in the visible spectrum. ACS Nano 2014;8(2):1809–16.
[68] Allen KW, Farahi N, Li Y, Limberopoulos NI, Walker Jr DE, Urbas AM, et al. Super-resolution microscopy by movable thin-films with embedded microspheres: resolution analysis. Ann Phys 2015;527(7–8):513–22.
[69] Darafsheh A, Limberopoulos NI, Derov JS, Walker Jr DE, Astratov VN. Advantages of microsphere-assisted super-resolution imaging technique over solid immersion lens and confocal microscopies. Appl Phys Lett 2014;104(6):061117.
[70] Allen KW, Farahi N, Li Y, Limberopoulos NI, Walker DE, Urbas AM, et al. Overcoming the diffraction limit of imaging nanoplasmonic arrays by microspheres and microfibers. Opt Express 2015;23(19):24484–96.
[71] Li PY, Tsao Y, Liu YJ, Lou ZX, Lee WL, Chu SW, et al. Unusual imaging properties of superresolution microspheres. Opt Express 2016;24 (15):16479–86.
[72] Wang F, Liu L, Yu H, Wen Y, Yu P, Liu Z, et al. Scanning superlens microscopy for non-invasive large field-of-view visible light nanoscale imaging. Nat Commun 2016;7:13748.
[73] Krivitsky LA, Wang JJ, Wang Z, Luk'yanchuk B. Locomotion of microspheres for super-resolution imaging. Sci Rep 2013;3:3501.
[74] Wu G, Hong M. Optical nano-imaging via microsphere compound lenses working in non-contact mode. Opt Express 2021;29(15):23073–82.
[75] Jia B, Li P, Wang F, Chan HY, Zhang G, Li WJ. Determination of microsphere-lens magnification using micro-robotic scanning superlens nanoscopy. IEEE Open J Nanotechnol. 2020;1:65–76.
[76] Huszka G, Yang H, Gijs MAM. Dielectric microsphere-based optical system for super-resolution microscopy. In: Proceedings of the 19th International Conference on Solid-State Sensors, Actuators and Microsystems (TRANSDUCERS); 2017 Jun 18–22; Kaohsiung, Taiwan. IEEE; 2017. p. 2003–6.
[77] Huszka G, Yang H, Gijs MAM. Microsphere-based super-resolution scanning optical microscope. Opt Express 2017;25(13):15079–92.
[78] Darafsheh A, Guardiola C, Palovcak A, Finlay JC, Cárabe A. Optical super-resolution imaging by high-index microspheres embedded in elastomers. Opt Lett 2015;40(1):5–8.
[79] Sasaki M, Kurosawa T, Hane K. Micro-objective manipulated with optical tweezers. Appl Phys Lett 1997;70(6):785–7.
[80] Mcleod E, Arnold CB. Subwavelength direct-write nanopatterning using optically trapped microspheres. Nat Nanotechnol 2008;3(7):413–7.
[81] Bañas A, Vizsnyiczai G, Búzás A, Palima D, Kelemen L, Ormos P, et al. Fabrication and optical trapping of handling structures for re-configurable microsphere magnifiers. In: Glückstad J, Andrews DL, Galvez EJ, editors. SPIE OPTO 2013: Proceedings Volume 8637, Complex Light and Optical Forces VII; 2013 Feb 2–7; San Francisco, CA, United States. SPIE; 2013. p. 135–39.
[82] Michihata M, Kim J, Takahashi S, Takamasu K, Mizutani Y, Takaya Y. Surface imaging technique by an optically trapped microsphere in air condition. Nanomanuf Metrol 2018;1:32–8.

[83] Liu X, Hu S, Tang Y, Xie Z, Liu J, He Y. Selecting a proper microsphere to combine optical trapping with microsphere-assisted microscopy. Appl Sci (Basel) 2020;10(9):3127.
[84] Zhou J, Lian Z, Zhou C, Bi S, Wang Y. Scanning microsphere array optical microscope for efficient and large area super-resolution imaging. J Opt 2020;22(10):105602.
[85] Zhang T, Li P, Yu H, Wang F, Wang X, Yang T, et al. Fabrication of flexible microlens arrays for parallel super-resolution imaging. Appl Surf Sci 2020;504:144375.
[86] Hao X, Kuang C, Li Y, Liu X, Ku Y, Jiang Y. Hydrophilic microsphere based mesoscopic-lens microscope (MMM). Opt Commun 2012;285(20):4130–3.
[87] Darafsheh A, Walsh GF, Dal Negro L, Astratov VN. Optical super-resolution by high-index liquid-immersed microspheres. Appl Phys Lett 2012;101 (14):141128.
[88] Lee S, Li L, Wang Z, Guo W, Yan Y, Wang T. Immersed transparent microsphere magnifying sub-diffraction-limited objects. Appl Opt 2013;52 (30):7265–70.
[89] Yang H, Gijs MAM. Optical microscopy using a glass microsphere for metrology of sub-wavelength nanostructures. Microelectron Eng 2015;143:86–90.
[90] Darafsheh A. Influence of the background medium on imaging performance of microsphere-assisted super-resolution microscopy. Opt Lett 2017;42 (4):735–8.
[91] Li S, Luo H, Liu F, Zhang T, Wang X, Liu L, et al. Imaging properties of microsphere superlenses with varying background refractive indices under inclined illumination. Opt Lett 2022;47(22):5857–60.
[92] Wang F, Yang S, Ma H, Shen P, Wei N, Wang M, et al. Microsphere-assisted super-resolution imaging with enlarged numerical aperture by semi-immersion. Appl Phys Lett 2018;112(2):023101.
[93] Du B, Ye YH, Hou J, Guo M, Wang T. Sub-wavelength image stitching with removable microsphere-embedded thin film. Appl Phys A 2016;122:15.
[94] Yang S, Wang X, Wang J, Cao Y, Wang F, Chen T, et al. Reduced distortion in high-index microsphere imaging by partial immersion. Appl Opt 2018;57 (27):7818–22.
[95] Zhou Y, Hong M. Realization of noncontact confocal optical microsphere imaging microscope. Microsc Res Tech 2021;84(10):2381–7.
[96] Cao Y, Yang S, Wang D, Wang J, Ye YH. Surface plasmon-enhanced dark-field microsphere-assisted microscopy. Opt Express 2023;31(5):8641–9.
[97] Hüser L, Pahl T, Künne M, Lehmann P. Microsphere assistance in interference microscopy with high numerical aperture objective lenses. J Opt Microsyst 2022;2(4):044501.
[98] Wang J, Jiang R, Yang S, Cao Y, Ye YH. Microsphere-assisted dark-field microscopy based on a fully immersed low refractive index microsphere. Opt Lett 2023;48(7):1858–61.
[99] Zhou Y, Tang Y, Deng Q, Zhao L, Hu S. Contrast enhancement of microsphere-assisted super-resolution imaging in dark-field microscopy. Appl Phys Express 2017;10(8):082501.
[100] Wang F, Lai HSS, Liu L, Li P, Yu H, Liu Z, et al. Super-resolution endoscopy for real-time wide-field imaging. Opt Express 2015;23(13):16803–11.
[101] Perrin S, Leong-Hoï A, Lecler S, Pfeiffer P, Kassamakov I, Nolvi A, et al. Microsphere-assisted phase-shifting profilometry. Appl Opt 2017;56 (25):7249–55.
[102] Wang F, Liu L, Yu P, Liu Z, Yu H, Wang Y, et al. Three-dimensional super-resolution morphology by near-field assisted white-light interferometry. Sci Rep 2016;6:24703.
[103] Aakhte M, Abbasian V, Akhlaghi EA, Moradi AR, Anand A, Javidi B. Microsphere-assisted super-resolved Mirau digital holographic microscopy for cell identification. Appl Opt 2017;56(9):D8–D13.
[104] Kassamakov I, Lecler S, Nolvi A, Leong-Hoï A, Montgomery P, Hæggström E. 3D super-resolution optical profiling using microsphere enhanced Mirau interferometry. Sci Rep 2017;7:3683.
[105] Leong-Hoi A, Hairaye C, Perrin S, Lecler S, Pfeiffer P, Montgomery P. High resolution microsphere-assisted interference microscopy for 3D characterization of nanomaterials. Phys Status Solidi A 2018;215 (6):1700858.
[106] Perrin S, Donie YJ, Montgomery P, Gomard G, Lecler S. Compensated microsphere-assisted interference microscopy. Phys Rev Appl 2020;13 (1):014068.
[107] Aljuaid W, Riley JA, Healy N, Pacheco-Peña V. On-fiber high-resolution photonic nanojets via high refractive index dielectrics. Opt Express 2022;30 (24):43678–90.
[108] Yang H, Cornaglia M, Gijs MAM. Photonic nanojet array for fast detection of single nanoparticles in a flow. Nano Lett 2015;15(3):1730–5.
[109] Li Y, Xin H, Liu X, Zhang Y, Lei H, Li B. Trapping and detection of nanoparticles and cells using a parallel photonic nanojet array. ACS Nano 2016;10 (6):5800–8.
[110] Li YC, Xin HB, Lei HX, Liu LL, Li YZ, Zhang Y, et al. Manipulation and detection of single nanoparticles and biomolecules by a photonic nanojet. Light Sci Appl 2016;5:e16176.
[111] Yang S, Ye YH, Zang J, Pei Y, Xia Y, Zhang J. Direct observation Brownian motion of individual nanoparticles in water using microsphere-assisted microscopy. Opt Lett 2021;46(13):3099–102.
[112] Stanescu SL, Vilain S, Galieni V, Goh G, Karpinska K, Barbolina I, et al. Imaging with the super-resolution microsphere amplifying lens (SMAL) nanoscope. In: Journal of Physics: Conference Series, Proceedings of Electron Microscopy and Analysis Group Conference 2017 (EMAG2017); 2017 Jul 3–6; Manchester, UK. IOP Publishing Ltd; 2017. p. 012014.
[113] Li G, Li P, Chen T, Tian X, Gao S, Yang Z, et al. Microspherical lens assembly for super-wide field of view of super-resolution optical imaging. In: Proceedings of the 20th International Conference on Nanotechnology (IEEE-NANO); 2020 Jul 29–31; Montreal, QC, Canada. IEEE; 2020. p. 168–71.
[114] Lee S, Li L. Rapid super-resolution imaging of sub-surface nanostructures beyond diffraction limit by high refractive index microsphere optical nanoscopy. Opt Commun 2015;334:253–7.
[115] Guo M, Ye YH, Hou J, Du B, Wang T. Imaging of sub-surface nanostructures by dielectric planer cavity coupled microsphere lens. Opt Commun 2017;383:153–8.
[116] Li L, Guo W, Yan Y, Lee S, Wang T. Label-free super-resolution imaging of adenoviruses by submerged microsphere optical nanoscopy. Light Sci Appl 2013;2:e104.
[117] Gao S, Meng K, Yang Z, Liu H, Wang F, Sun L, et al. The probe-combined microspheres applied in biomedical field for super-resolution imagings and micromanipulations. In: Proceedings of the 4th Asia-Pacific Conference on Intelligent Robot Systems (ACIRS); 2019 Jul 13–15; Nagoya, Japan. IEEE; 2019. p. 155–58.
[118] Jia B, Wang F, Chan H, Zhang G, Li WJ. In situ printing of liquid superlenses for subdiffraction-limited color imaging of nanobiostructures in nature. Microsyst Nanoeng 2019;5:1.
[119] Zhang Q, Li J, Pan X, Liu X, Gai H. Low-numerical aperture microscope objective boosted by liquid-immersed dielectric microspheres for quantum dot-based digital immunoassays. Anal Chem 2021;93(38):12848–53.
[120] Wu G, Ng SWL, Zhou Y, Hong M. Dynamic nano-imaging via a microsphere compound lens integrated microfluidic device with a 10× objective lens. Lab Chip 2023;23(13):3070–9.
[121] Jin G, Hong S, Rich J, Xia J, Kim K, You L, et al. Intelligent nanoscope for rapid nanomaterial identification and classification. Lab Chip 2022;22 (16):2978–85.
[122] Anderson PW. More is different: broken symmetry and the nature of the hierarchical structure of science. Science 1972;177(4047):393–6.
[123] Zhang Y, Gross H. Systematic design of microscope objectives. Part II: Lens modules and design principles. Adv Opt Technol 2019;8(5):349–84.
[124] Kim D, Choi H, Brendel T, Quach H, Esparza M, Kang H, et al. Advances in optical engineering for future telescopes. Opto-Electron Adv 2021;4 (6):210040.
[125] Lai HSS, Wang F, Li Y, Jia B, Liu L, Li WJ. Super-resolution real imaging in microsphere-assisted microscopy. PLoS One 2016;11(10):e0165194.
[126] Astratov VN, Jin B, Erykalin AA, Maslov AV. Ball lens-assisted smartphone microscopy with diffraction-limited resolution. In: Lecler S, Astratov VN, Minin IV, editors. SPIE Photonics Europe 2022: Proceedings Volume 12152, Mesophotonics: Physics and Systems at Mesoscale; 2022 Apr 3–May 23; Strasbourg, France. SPIE; 2022. p. 31–6.
[127] Zhou J, Zeng B, Bi S, Wang Y. Enhanced magnification factors in super-resolution imaging using stacked dual microspheres. J Opt 2020;22 (8):085605.
[128] Luo H, Yu H, Wen Y, Zhang T, Li P, Wang F, et al. Enhanced high-quality super-resolution imaging in air using microsphere lens groups. Opt Lett 2020;45 (11):2981–4.
[129] Deng Y, Yang S, Xia Y, Cao Y, Wang J, Wang F, et al. Super-resolution imaging properties of cascaded microsphere lenses. Appl Opt 2018;57(20): 5578–82.
[130] Zhu H, Yan B, Zhou S, Wang Z, Wu L. Synthesis and super-resolution imaging performance of a refractive-index-controllable microsphere superlens. J Mater Chem C 2015;3(41):10907–15.
[131] Dhama R, Yan B, Palego C, Wang Z. Super-resolution imaging by dielectric superlenses: TiO_2 metamaterial superlens versus $BaTiO_3$ superlens. Photonics 2021;8(6):222.
[132] Zhu H, Fan W, Zhou S, Chen M, Wu L. Polymer colloidal sphere-based hybrid solid immersion lens for optical super-resolution imaging. ACS Nano 2016;10 (10):9755–61.
[133] Fan W, Yan B, Wang Z, Wu L. Three-dimensional all-dielectric metamaterial solid immersion lens for subwavelength imaging at visible frequencies. Sci Adv 2016;2(8):e1600901.
[134] Yan B, Wang Z, Parker AL, Lai Y, Thomas PJ, Yue L, et al. Superlensing microscope objective lens. Appl Opt 2017;56(11):3142–7.
[135] Huszka G, Gijs MAM. Turning a normal microscope into a super-resolution instrument using a scanning microlens array. Sci Rep 2018;8:601.
[136] Yan B, Song Y, Yang X, Xiong D, Wang Z. Unibody microscope objective tipped with a microsphere: design, fabrication, and application in subwavelength imaging. Appl Opt 2020;59(8):2641–8.
[137] Vlad A, Huynen I, Melinte S. Wavelength-scale lens microscopy via thermal reshaping of colloidal particles. Nanotechnology 2012;23(28):285708.
[138] Du B, Zhang H, Xia J, Wu J, Ding H, Tong G. Super-resolution imaging with direct laser writing-printed microstructures. J Phys Chem A 2020;124 (35):7211–6.
[139] Wu G, Zhou Y, Hong M. Sub-50 nm optical imaging in ambient air with 10× objective lens enabled by hyper-hemi-microsphere. Light Sci Appl 2023;12:49.
[140] Lee JY, Hong BH, Kim WY, Min SK, Kim Y, Jouravlev MV, et al. Near-field focusing and magnification through self-assembled nanoscale spherical lenses. Nature 2009;460(7254):498–501.

[141] Song S, Li Y, Yao Z, Li J, Li X, Cao Y. 3D laser nanoprinting of optically functionalized structures with effective-refractive-index tailorable TiO_2 nanoparticle-doped photoresin. Nanomaterials 2022;12(1):55.
[142] Kang D, Pang C, Kim SM, Cho HS, Um HS, Choi YW, et al. Shape-controllable microlens arrays via direct transfer of photocurable polymer droplets. Adv Mater 2012;24(13):1709–15.
[143] Li P, Yu H, Wen Y, Zhao W, Liu L, Li WJ. Direct transfer printing of dielectric nanoparticle assembled superlens array for super-resolution imaging. In: Proceedings of the 19th International Conference on Nanotechnology (IEEE-NANO); 2019 Jul 22–26; Macao, China. IEEE; 2019. p. 405–9.
[144] Shang Q, Tang F, Yu L, Oubaha H, Caina D, Yang S, et al. Super-resolution imaging with patchy microspheres. Photonics 2021;8(11):513.
[145] Zhu H, Chen Z, Chong TC, Hong M. Photonic jet with ultralong working distance by hemispheric shell. Opt Express 2015;23(5):6626–33.
[146] Shen Y, Wang LV, Shen JT. Ultralong photonic nanojet formed by a two-layer dielectric microsphere. Opt Lett 2014;39(14):4120–3.
[147] Zhou Y, Hong M. Formation of a three-dimensional bottle beam via an engineered microsphere. Photon Res 2021;9(8):1598–606.
[148] Zhou Y, Hong M. Formation of polarization-dependent optical vortex beams via an engineered microsphere. Opt Express 2021;29(7):11121–31.
[149] Zhou Y, Ji R, Teng J, Hong M. Wavelength-tunable focusing via a Fresnel zone microsphere. Opt Lett 2020;45(4):852–5.
[150] Wu M, Huang B, Chen R, Yang Y, Wu J, Ji R, et al. Modulation of photonic nanojets generated by microspheres decorated with concentric rings. Opt Express 2015;23(15):20096–103.
[151] Wu M, Chen R, Soh J, Shen Y, Jiao L, Wu J, et al. Super-focusing of center-covered engineered microsphere. Sci Rep 2016;6:31637.
[152] Zhou Y, Ji R, Teng J, Hong M. Ultralong light focusing via negative axicon microsphere. Eng Res Express 2020;2(1):015044.
[153] Liao M, Zheng S, Pan S, Lu D, He W, Situ G, et al. Deep-learning-based ciphertext-only attack on optical double random phase encryption. Opto-Electron Adv 2021;4(5):200016.
[154] Guo Y, Zhong L, Min L, Wang J, Wu Y, Chen K, et al. Adaptive optics based on machine learning: a review. Opto-Electron Adv 2022;5(7):200082.